DEMONSTRATION REPORT

Dipole Discrimination Techniques Applied to Live Sites Camp Ellis

ESTCP Project MR-201226

JULY 2014

Leonard Pasion
Black Tusk Geophysics Inc.

Distribution Statement A

This document has been cleared for public release

Executive Summary

The demonstration described in this report was conducted at Camp Ellis, Illinois, under project ESTCP MR-201226 “Dipole Discrimination Techniques Applied to Live Sites.” It was performed under the umbrella of the ESTCP Live-Site Classification Study Program. The objective of the MR-201226 project is to demonstrate the application of feature extraction and statistical classification to the problem of UXO discrimination. At the Camp Ellis site, the objective was to discriminate targets of interest (TOI) (including 2.36-inch practice rockets targets, a range of hand and rifle grenades as well as industry standard objects (ISOs)) from non-hazardous shrapnel, range and cultural debris. In this report, we describe the performance of classification techniques that utilized cued interrogation style data acquired with MetalMapper and TEMTADS 2x2 sensors processed by analysts from Black Tusk Geophysics (BTG) and the University of British Columbia Geophysical Inversion Facility (UBC-GIF).

The classification techniques applied to the Camp Ellis data used dipole model-based features extracted from observed data around each anomaly. One, two and three source dipole inversions were carried out for all data sets. From the extracted feature vectors, prioritized dig-lists were created for: (i) MetalMapper cued and (ii) TEMTADS 2x2 static/cued data. Dig lists were generated using a combination of size/decay and a library matching method comparing polarizabilities estimated via inversion at each target location with reference polarizabilities from test pit, training data and a library of polarizabilities from different sites. All model fits and discrimination analyses were performed using the classification software suite (UXOLab) that was jointly developed by UBC-GIF and Black Tusk Geophysics.

MetalMapper and TEMTADS 2x2 data were acquired by ARCADIS. In order to preserve the integrity of the blind-test, and to provide a comparison between the different processing methods, a unique analyst was assigned to process each data set. In this way, ground truth obtained as part of processing data with a particular method would not be shared with a different classification approach. For each dig-list, an objective classification method was applied to the features to construct the dig-list. Analysts were instructed to avoid "expert input" when constructing the dig-list. The dig order was determined automatically, and analysts did not manually change the position of any anomaly within a list based on visual inspection of the polarizabilities (i.e. manual labeling of anomalies as TOI or non-TOI).

The application of library classification methods to the MetalMapper and TEMTADS 2x2 datasets resulted in 98.4% and 97.4% of TOI identified respectively. In both cases the same TOI, EL-941, a rifle grenade at 19cm, was missed. Retrospective analysis identifies scenarios where the missed TOI could have been identified while also recognizing that EL-941 was missing part of the head and the entire tail fin section and produced polarizabilities that more closely matched the non-TOI rocket motor making it a particularly challenging target. At the stop dig point, 15.6% of non-TOI was dug for the MetalMapper and 14.4% was dug for the TEMTADS 2x2. There are a number of conclusions from applying dipole-based classification techniques to the Camp Ellis demonstration. The comparable classification results for MetalMapper and TEMTADS 2x2 datasets illustrates the sensor independent nature of the processing algorithms and classification methodologies, however the common missed TOI illustrates the challenge of sites where there are subtle differences in the recovered polarizabilities for TOI and non-TOI.

Table of Contents

Executive Summary i

Table of Contents ii

List of Tables iv

List of Figures iv

Acronyms viii

1.0 INTRODUCTION 1

1.1 Background 1
1.2 Objective of the Demonstration 2
1.3 Regulatory Drivers 2
2.0 TECHNOLOGY 3

2.1 Technology Description 3
2.2 UXOLab Software 5
2.3 Previous Testing of the Technology 6
2.4 Advantages and Limitations of the Technology 7
3.0 PERFORMANCE OBJECTIVES 8

3.1 Objective: Detection of all TOI 10
3.2 Objective: Maximize Correct Classification of TOI 10
3.3 Objective: Maximize Correct Classification of non-TOI 11
3.4 Objective: Specification of no-dig Threshold 11
3.5 Objective: Minimize Number of Anomalies that Cannot be Analyzed 12
3.6 Objective: Correct Estimation of Target Parameters 12
4.0 SITE DESCRIPTION 12

5.0 TEST DESIGN 12

6.0 DATA ANALYSIS AND RESULTS 13

6.1 Cued MetalMapper Results 16
6.2 Cued TEMTADS 2x2 20
7.0 MANAGEMENT AND STAFFING 22

8.0 REFERENCES 23

9.0 APPENDICES 24

Appendix A: MetalMapper Feature Extraction and Classification 25
Appendix B: MetalMapper Polarizability Match to Targets of Interest 42

Appendix C: MetalMapper Location and Depth Error Estimates 46
Appendix D: TEMTADS 2x2 Feature Extraction and Classification 47
Appendix E: TEMTADS 2x2 Polarizability Match to Targets of Interest 58
Appendix F: TEMTADS 2x2 Depth Error Estimates..... 61
Appendix G: Points of Contact 62

List of Tables

Table 1: Performance Objectives for the Camp Ellis demonstration. 8
Table 2: Performance Objectives for the Camp Ellis demonstration with sensor specific results for Metalmapper and TEMTADS 2x2. 9
Table 3: Summary of classification performance for Camp Ellis MetalMapper and TEMTADS 2x2 datasets 15
Table 4. List of missed QC seeds. 31
Table 5: List of ordnance items in the reference library used in creating the final dig list 34
Table 6: Recovered polarizability accuracies relative to the best matching reference library item for Camp Ellis MetalMapper dataset. 45
Table 7: TEMTADS 2x2 Evaluation of Matching Levels at Camp Ellis 47
Table 8: Summary of TEMTADS 2x2 classification result at Camp Ellis. 51
Table 9: Recovered polarizability accuracies relative to the best matching reference library item for TEMTADS 2x2. 60

List of Figures

Figure 1: Previous Inversion/Classification Testing: A list of sites where classification has been applied and the types of sensor data that have been analyzed at each site. Green X's denote instances where industry geophysicists have processed datasets using UXOLab software after receiving training from BTG staff. 6
Figure 2: ROC curves and relevant classification statistics used to compute the metrics for the MetalMapper and TEMTADS 2x2 as listed in Table 2. 10
Figure 3: MetalMapper Dynamic data used to identify potential targets. The vertical component of the middle three cubes are gridded to form the image. An approximately 150 m x 200 m region of the former rocket, rifle grenade and hand grenade range was mapped with the MetalMapper. A high density region at the center of the map was also mapped by the TEMTADS 2x2 in a dynamic mode (red rectangle). On the right is a close-up of the region in the red rectangle. 13
Figure 4: Camp Ellis cued data locations for MetalMapper and TEMTADS 2x2. In (a) and (b), the red dots represent targets of interest and non-TOI are represented by white '+' symbols. In (c), the red dots in the northern portion correspond to cued TEMTADS 2x2 measurements, blue dots in the south represent cued MetalMapper measurements while the black dots in the central region are locations where measurements were made with both sensors. 14
Figure 5: Overview of workflow applied to each dataset from Camp Ellis. 15
Figure 6: MetalMapper sensor collecting data at Camp Beale. Sensor consists of three orthogonal transmitters and seven multi-static receiver cubes. 16
Figure 7: Polarizabilities for a cluster of self-similar polarizabilities identified with BTG's *TrainZilla* software. Colored lines are predicted polarizabilities. Broken grey lines are best fitting reference polarizabilities. Training data were requested for Anomalies EL-658 andEL-742 (stars); ground truth (photos) revealed that both of these anomalies are non-TOI (2.36" rocket bodies/weights (also metal debris in EL-658). 17
Figure 8: Decay versus size feature space plot showing passed models (blue dots) and the location of training data requests (red dots). Stars are library reference items. 17
Figure 9: Final ROC curve for cued MetalMapper data from Camp Ellis. 19

Figure 10: Top: polarizabilities for missed TOI EL-941 (colored lines), a rifle grenade at 19 cm depth, and the best fitting rifle grenade reference polarizabilities ("Steel RG D", which were based on EL-132: broken grey lines). Bottom Left: ground truth photo for El-941. Note that the rifle grenade is not intact. Bottom Right: ground truth photo for EL-132. Note that this rifle grenade is intact. 19
Figure 11: The TEMTADS 2x2 instrument being operated at the Former Spencer Artillery Range 20
Figure 12: Selected training data requests all of which were revealed to be non-TOI including: (a) munitions debris (EL-812) and (b, c) 2.36" rocket motors (EL-752, EL-1180). 20
Figure 13: Final ROC curve for cued TEMTADS 2x2 data from Camp Ellis. 21
Figure 14: Project management hierarchy showing BTG personnel in blue and UBC-GIF personnel in green. The hierarchy is split between the development and execution components.22
Figure 15: Example of an unrealistic 2OI model (anomaly 1250; frag). The first model of the 2OI (model 2) provides the best fit (i.e., minimum misfit) to the reference polarizabilities (misfit = 0.746), but the predicted depth of 1.2m and location at the edge of the instrument (i.e., at the vertical and horizontal inversion boundaries), and high amplitude and jittery appearance of the polarizabilities are classic signs that this model is an artifact of the multi-object inversion process. Accordingly, this model was failed during QC. Polarizabilities for SOI and 2OI are shown at left. Modeled target locations (X-Y and Z) are shown at the top right (gridded EM61 data is displayed behind the X-Y plot). Gridded observed, predicted and residual data for SOI and 2OI are shown below location maps. Decay versus size feature plot is shown in bottom right. Dots are test data; stars are reference items. Numbered circles are models for this anomaly. 26
Figure 16: Distribution of passed models in decay(t1,t29) versus size(t1) feature space, where size(t1) is the total polarizability measured at the first time channel (t1=0.106ms), and decay(t1,t29) is size(t1)/size(t29) where t29=2.006ms. Some outliers are not shown. Labeled stars represent ordnance library reference items. 27
Figure 17: Example of use of the training data selection tool (*TrainZilla*). A polygon (solid black line) is drawn in feature space. Clusters of items with self-similar polarizabilities are automatically found based on the specified cluster search parameters. In this case a cluster comprising 7 features is visible (solid feature symbols encompassed by broken line). Polarizabilities for this cluster are shown in Figure 18. 28
Figure 18: Polarizabilities for the cluster shown in Figure 17. Colored lines are predicted polarizabilities. Broken grey lines are best fitting reference polarizabilities. Training data were requested for Anomalies EL-658 andEL-742 (stars); ground truth (photos) revealed that both of these anomalies are non-TOI (2.36" rocket bodies/weights (also metal debris in EL-658). 28
Figure 19: Decay versus size feature space plot showing passed models (blue dots) and the location of training data requests (red dots). Stars are library reference items. Broken black line outlines a region of high feature density. 29
Figure 20: Screen shot of the UXOLab *DigZilla* graphical user interface. Features in the decay versus size feature plot are color coded according to dig list order. 30
Figure 21: Polarizabilities for EL-132 (rifle grenade; red, black and magenta lines) relative to polarizabilities for the steel rifle grenade reference item from test pit measurements (broken grey lines). 31
Figure 22: (a) Polarizabilities for EL-1522 (2.36" rocket) relative to polarizabilities for the 2.36" rocket reference item from test pit measurements. (b) Ground truth photo for EL-1522. (c) Ground truth photo for EL-1719. 32

Figure 23: Left: polarizabilities and ground truth for EL-1522 (2.36" rocket). Right: polarizabilities and ground truth for EL-1517 (2.36" rocket motor). 33
Figure 24: Partial ROC curve for the stage 2 dig list. 34
Figure 25: Ordnance library used to create the final (stage 3) dig list. 35
Figure 26: Partial ROC curve for the stage 3 (final) dig list. 36
Figure 27: Final ROC curve. One missed TOI (EL-941, rifle grenade 19cm deep) was dug at dig number 587. 36
Figure 28: Left: polarizabilities for missed TOI EL-941 (colored lines), a rifle grenade at 19 cm depth, and the best fitting rifle grenade reference polarizabilities ("Steel RG D", which was based on EL-132: broken grey lines). Center: ground truth photo for El-941. Note that the rifle grenade is not intact. Right: ground truth photo for EL-132. Note that this rifle grenade is intact. 37
Figure 29: Polarizabilities for missed QC seed EL-132 (colored lines) plotted against the best fitting reference items available during the creation of the stage 1 dig list. Top left: SOI model; Top center and right: 2OI models; Bottom row: 3OI models. Models highlighted in red show the models that were used to construct our "Steel RG D" reference item. If instead we had created a reference model based on the SOI model (highlighted in blue), EL-941 would have been dug much earlier. 38
Figure 30: Polarizabilities for missed TOI EL-941 (colored lines) plotted against a reference item ("Steel RG E") based on the SOI model for EL-132. 38
Figure 31: Polarizabilities for 32 small ISOs at Camp Ellis. Colored lines are predicted polarizabilities. Broken grey lines are small ISO reference polarizabilities taken from IVS measurements. Anomaly ID is the number after the "T" in each label. Polarizabilities are sorted by misfit (from best to worst) with respect to the small ISO reference model. 40
Figure 32: Compilations of polarizabilities for small ISOs from recent Live Site demonstrations. The two Beale and Spencer datasets each comprise the same set of anomalies but the data were collected by two different companies. The Spencer data include small ISOs from both the Open and Dynamic Areas. Misfit values are the mean misfits with respect to the reference polarizabilities calculated over all time channels using all three polarizabilities (L1, L2 and L3). 41
Figure 33: MetalMapper polarizability matching to TOI. The grey curve represents the TOI polarizabilities from the reference library and the red curve depicts the best matching recovered polarizabilities. The title of each plot lists the ground truth as well as the percent error between the library reference item and the recovered polarizabilities. 42
Figure 34: MetalMapper polarizability matching to TOI. The grey curve represents the TOI polarizabilities from the reference library and the red curve depicts the best matching recovered polarizabilities. The title of each plot lists the ground truth as well as the percent error between the library reference item and the recovered polarizabilities. 43
Figure 35: MetalMapper polarizability matching to TOI. The grey curve represents the TOI polarizabilities from the reference library and the red curve depicts the best matching recovered polarizabilities. The title of each plot lists the ground truth as well as the percent error between the library reference item and the recovered polarizabilities. 44
Figure 36: Location and depth error distributions. 46
Figure 37: The polarizabilities of some suspicious anomalies in the training stage, War head: (a)-(c), rocket motor: (d)-(f) and rocket weight: (g)-(h). 48

Figure 38: Seven reference classes used in the library matching method for the classification of TEMTADS 2x2 data at Camp Ellis. 49
Figure 39: Polarizabilities of six TOI found in the training stage. Small ISO: (a)-(b). Hand Grenade: (c)-(e). Rifle Grenade: (f). 50
Figure 40: Final ROC curve (stage 4) for TEMTADS 2x2 cued data. One TOI was missed. 51
Figure 41: Missed QC seed EL-143: (a) Ground truth photo; (b) The test polarizabilities (red and blue curves) used for classification (grey curve is best matching library reference named RktMtrA); (c) the best matching polarizabilities for EL-143 that match the hand grenade reference polarizabilities; (d)-(e): recovered polarizabilities for two different targets (EL-87, EL-55) which provided high quality matches to the reference hand grenade. (f)-(g): Two other requested training anomalies (EL-970, EL-512 (non-TOIs) with polarizabilities similar to those shown for EL-143 in (c) relative to the library reference hand grenade. 53
Figure 42: Polarizabilities of training anomalies (a) –(c) which were revealed to be munitions debris (EL-812) and 2.36" rocket motors (EL-752, EL-1180) and the two digs (d)-(e) in stage 1 similar to the missed QC seed EL-143 (f). Ground truth showed that none of the targets in (a)-(e) were TOI, leading to the decision to consider (f) a likely non-TOI rocket motor. 54
Figure 43: Missed QA seed EL-941 and related, similar non-TOI. (a) El-941 photo. (b) Test polarizabilities (red and blue curves) used for classification and best matching referenceitem (RktMtrC). (c)-(h) Similar non-TOI anomalies adjacent to EL-941. (i)-(k) non-TOI training anomalies with a slow decay after 3 ms relative to anomalies in (b)-(h). 56
Figure 44: A Rifle Grenade class group obtained after removing RktMtrC from the reference library: EL-417, missed QA seed EL-941 and EL-607 are marked as the first three "rGrenade" anomalies. They would most likely be requested as the most "suspicious Grenade" anomalies in the training process. Thus EL-941 would be caught at the expense of digging a few more non-TOI. 57
Figure 45: TEMTADS 2x2 polarizability matching to TOI. The grey curve represents the TOI polarizabilities from the reference library and the red curve depicts the best matching recovered polarizabilities. The title of each plot lists the ground truth as well as the percent error between the library reference item and the recovered polarizabilities. 58
Figure 46: TEMTADS 2x2 polarizability matching to TOI. The grey curve represents the TOI polarizabilities from the reference library and the red curve depicts the best matching recovered polarizabilities. The title of each plot lists the ground truth as well as the percent error between the library reference item and the recovered polarizabilities. 59
Figure 47: TEMTADS 2x2 depth error estimates for Camp Ellis. The bias in the depth errors is assumed to be a consequence of the sensor height used in the inversions differing from the actual sensor height. 61

Acronyms

EM	Electromagnetic
EMI	Electromagnetic induction
ESTCP	Environmental Security Technology Certification Program
FAR	False alarm rate
IDA	Institute for Defense Analyses
IMU	Inertial Measurement Unit
ISO	Industry standard object
IVS	Instrument verification strip
PI	Principal Investigator
PNN	Probabilistic Neural Network
POC	Point of Contact
QC	Quality Control
ROC	Receiver operating characteristic
SERDP	Strategic Environmental Research and Development Program
SLO	San Luis Obispo
SNR	Signal to noise ratio
SOI	Single object inversion
TEMTADS	Time Domain Electromagnetic Towed Array Detection System
TOI	Target of interest
UBC-GIF	University of British Columbia – Geophysical Inversion Facility
UBC	University of British Columbia
USACE ERDC	United States Army Corps of Engineers- Engineering Research and Development Center
UXO	Unexploded ordnance
2OI	Two Object Inversion
3OI	Three Object Inversion

1.0 INTRODUCTION

1.1 Background

Significant progress has been made in discrimination technology. To date, testing of these approaches has been primarily limited to test sites with only limited application at live sites. Acceptance of discrimination technologies requires demonstration of system capabilities at real UXO sites under real world conditions. Any attempt to declare detected anomalies to be harmless and requiring no further investigation will require demonstration to regulators of not only individual technologies, but an entire decision making process.

To demonstrate the viability of advanced detection and discrimination technologies, ESTCP has now conducted four UXO classification studies. The results of the first demonstration, at the former Camp Sibert, Alabama were very encouraging. Although conditions were favorable at this site, including a single target-of-interest (4.2-in mortar) and benign topography and geology, all of the demonstrated classification approaches were able to correctly identify a sizable fraction of the anomalies as arising from non-hazardous items that could be safely left in the ground. Of particular note, the contractor EM-61-MK2 cart survey with analysis using commercially available methods correctly identified more than half the targets as non-hazardous.

To build upon the success of this first study, ESTCP expanded the program to include a second study at a site with more challenging topography and a wider mix of targets-of interest. A range at the former Camp San Luis Obispo (SLO), California, was selected for this demonstration. We again found that, with appropriate use of classification metrics applied to production quality EM-61 data, it was possible to significantly reduce the number of clutter items excavated without missing any targets of interest (TOI). Furthermore, the next generation of EM sensors, when deployed in a cued-interrogation mode, produced significant additional reductions in the number of clutter items excavated. These sensors could also usually distinguish between different UXO types. A third ESTCP demonstration study was conducted in 2010 at Camp Butner, North Carolina. The site had very little topographic relief but required classification between small targets of interest (37mm projectiles and M48 fuzes) and metallic debris of similar size. Targets were also distributed with a higher density than previously encountered. In 2011, an additional ESTCP demonstration study was conducted at Camp Beale, California. The site had very little topographic relief but required classification between small targets of interest (37mm projectiles and M48 fuzes) and metallic debris of similar size. Targets were also distributed with a higher density than previously encountered. In 2012 an ESTCP demonstration was performed at Spencer Range in Tennesee which included the challenge of two large one off items (105mm, 155mm) as well as the seeding of multi object scenarios where varying sized pieces of clutter were placed nearby a TOI.

Results are presented here for the ESTCP demonstration study conducted in 2012 at Camp Ellis, Illinois. The ranges of targets of interest present included 2.36-inch rockets, hand and rifle grenades in addition to small ISOs. This demonstration report describes the data processing, feature extraction and classification that were conducted by Black Tusk Geophysics (BTG) and the University Of British Columbia (UBC) on the Camp Ellis data sets.

1.2 Objective of the Demonstration

The objectives of this demonstration were to perform data modeling, classification, and classification using electromagnetic (EM) data collected by the various data collection demonstrators participating in the study. Specifically, we processed the following datasets collected at Camp Ellis:

1) TEMTADS 2x2 cued interrogation array data; and
2) MetalMapper cued interrogation data (all data acquired by ARCADIS);

Specific processing tasks were as follows:

1) Feature Extraction: inversion of all electromagnetic data sets with a three dipole instantaneous amplitude model
2) Classification: the following ranked dig sheets for Camp Ellis:

    a) Cued TEMTADS 2x2 polarization match: A digsheet was produced based on how well the recovered polarization matched the polarizations in a library of ordnance items expected at the site.

    b) Cued MetalMapper polarization match: A digsheet was produced based on how well the recovered polarization matched the polarizations in a library of ordnance items expected at the site;

Thus we produced two ranked dig sheets, one for each of the MetalMapper and TEMTADS 2x2 datasets.

1.3 Regulatory Drivers

Refer to the Program Office demonstration plan for a discussion of regulatory drivers.

2.0 TECHNOLOGY

2.1 Technology Description

Magnetic and EM methods represent the main sensor types used for detection of UXO. Over the past 10 years, significant research effort has been focused on developing methods to discriminate between hazardous UXO and non-hazardous scrap metal, shrapnel and geology (e.g. Bell et al., 2001; Pasion et al., 2007; Tantum et al., 2008; Liao and Carin, 2009). The most promising classification methods typically proceed by first recovering a set of parameters that specify a physics-based model of the object being interrogated. For example, in time-domain electromagnetic (TEM) data, the parameters comprise the object location and the polarization tensor (typically two or three collocated orthogonal dipoles along with their orientation and some parameterization of the time-decay curve). For magnetics, the physics based model is generally a static magnetic dipole. Once the parameters are recovered by inversion, a subset of the parameters is used as feature vectors to guide either a statistical or rule-based classifier.

Magnetic and EM phenomenologies have different strengths and weaknesses. Magnetic data are simpler to collect, are mostly immune to sensor orientation and are better able to detect deeper targets. EM data are sensitive to non-ferrous metals, are better at detecting smaller items and are able to be used in areas with magnetic geology. Only EM data was acquired at Camp Ellis and in the remainder of this report we therefore focus on EM sensing and processing.

There are three key elements that impact the success of the UXO classification process described in the previous paragraphs:

1) Creation of a map of the geophysical sensor data: This includes all actions required to form an estimate of the geophysical quantity in question (i.e. amplitude of EMI response at a given time-channel) at each of the visited locations. The estimated quantity is dependent on the following:
    a. Hardware, including the sensor type, deployment platform, position and orientation system and the data acquisition system used to record and time-stamp the different sensors;
    b. Survey parameters such as line spacing, sampling rate, calibration procedures etc.;
    c. Data processing such as merging of position/orientation information with sensor data, noise and background filtering applied;
    d. The background environment including geology, vegetation, topography, cultural features, etc.; and
    e. Depth and distribution of ordnance and clutter.
2) Anomaly selection and feature extraction: This includes the detection of anomalous regions and the subsequent extraction of a polarization tensor model for each anomaly.
3) Classification of anomalies: The final objective of the demonstration is the production of a dig sheet with a ranked list of anomalies. This can be achieved via statistical classification which will require training data to determine the attributes of the UXO and non-UXO classes.

The focus of this demonstration is on the further testing and validation of the methodologies for 2) and 3) above that have been developed in UXOLab jointly by BTG and UBC-GIF. We now describe each of the three key elements of the technology as identified above.

Creation of a Map of Geophysical Sensor Data

At Camp Ellis, a list of target picks consisting of cued measurement locations for the MetalMapper and TEMTADS 2x2 were delivered from the Program Office. BTG did not analyze any of the dynamic data for the Camp Ellis demonstration (decision was made in conjunction with the Program Office to rather process the dynamic MetalMapper and TEMTADS 2x2 data from Camp Ellis as part of SERDP MR-2318).

Anomaly Selection and Feature Extraction

At this point in the process flow, there is a map of each of the geophysical quantities measured during the survey. The next step in the process is detection of anomalous regions followed by the extraction of features for each of the detected items. For this demonstration, targets have been picked from the MetalMapper dynamic data by the demonstrator, no additional picks were made by BTG/UBC-GIF.

In the EMI method, a time varying field illuminates a buried, conductive target. Currents induced in the target then produce a secondary field that is measured at the surface. EM data inversion involves using the secondary field generated by the target for recovery of the position, orientation, and parameters related to the target's material properties and shape. In the UXO community, the inverse problem is simplified by assuming that the secondary field can be accurately approximated as a dipole. In general, TEM sensors use a step off field to illuminate a buried target. The currents induced in the buried target decay with time, generating a decaying secondary field that is measured at the surface. The time-varying secondary magnetic field $\mathbf{B}(t)$ at a location $\mathbf{r}$ from the dipole $\mathbf{m}(t)$ is computed as:

$$\mathbf{B}(t) = \frac{\mu_O}{4\pi r^3}\mathbf{m}(t)\cdot\left(3\hat{\mathbf{r}}\hat{\mathbf{r}} - \overline{\overline{\mathbf{I}}}\right) \tag{1}$$

where $\hat{\mathbf{r}} = \mathbf{r}/|\mathbf{r}|$ is the unit-vector pointing from the dipole to the observation point, $\mathbf{I}$ is the 3 x 3 identity matrix, $\mu_o = 4\ \pi \times 10^{-7}$ H/m is the permittivity of free space and $r = |\mathbf{r}|$ is the distance between the center of the object and the observation point.

The dipole induced by the interaction of the primary field $\mathbf{B}_o$ and the buried target is given by:

$$\mathbf{m}(t) = \frac{1}{\mu_O}\overline{\overline{\mathbf{M}}}(t)\cdot\mathbf{B}_O \tag{2}$$

The induced dipole is the projection of the primary field $\mathbf{B}_o$ onto the target's polarizability tensor $\mathbf{M(t)}$. The polarizability tensor is assumed to be symmetric and positive definite and so can be decomposed as

$$\boldsymbol{M}(t) = \boldsymbol{A}^T\mathbf{L}(t)\boldsymbol{A} \tag{3}$$

with $\boldsymbol{A}$ an orthogonal matrix which rotates the coordinate system from geographic coordinates to a local, body centered coordinate system. The diagonal eigenvalue matrix $\mathbf{L}$(t) contains the principal polarizabilities L_i(t) (i = 1, 2, 3), which are assumed to be independent of target orientation and location. Features derived from the dipole model, in particular amplitude and decay of the principal polarizabilities, have been successfully used to discriminate between targets of interest and non-hazardous metallic clutter. These parameters are useful because, to first order, a conductor can be modeled as a simple LR loop which is inductively coupled to transmitters and receivers on the surface. The current response of this loop is a decaying exponential which is fully described by an amplitude and time constant (West and Macnae, 1991). The TEM dipole model generalizes this simple circuit model to account for target size and shape.

This latter property is represented by the principal polarizabilities, which decay independently in time and are approximately aligned with the semi-major and minor axes of the target.

Equal transverse (secondary and tertiary) polarizabilities indicate an axisymmetric target. Most ordnance can be treated as bodies of revolution (Shubitidze et al., 2002), and so equality of transverse polarizabilities has been proposed as a useful feature for discriminating between TOI and irregularly-shaped clutter. However, in practice it has been difficult to reliably estimate target shape using data from mono-static, vertical-component sensors conventionally deployed for UXO detection. This is because monostatic data often cannot adequately interrogate the transverse response of buried targets.

Recent advances in TEM sensor technology for UXO detection have helped address these limitations. For example, the MetalMapper sensor is comprised of an array of 7 receivers that measure 3 orthogonal components of the secondary field generated by 3 orthogonal transmitter loops that are fired sequentially. This multi-static, and multi-transmitter configuration provides a very rich data set which is better able to constrain target depth and transverse polarizabilities than a mono-static sensor.

When solving parametric inverse problems, it is usually sufficient to minimize a data norm quantifying the misfit between observed (dobs) and predicted data

$$\phi_d = \left\| V_d^{-1/2}\left(d^{obs} - d^{pred}\right)\right\|^2 \qquad (4)$$

with $d^{pred} = F(m)$ generally a nonlinear functional of the model m, and $Vd^{-1/2}$ a (usually diagonal) covariance matrix specifying estimated errors on the data. Bound constraints are also typically imposed to ensure that physically reasonable model parameters are obtained (e.g. polarizabilities should be positive). In the case of TEM data, the model is parameterized in terms of target location and orientation, as well as principal polarizabilities at each time channel. Equation 4 is minimized by first estimating the target location, followed by estimating of polarizabilities at each time channel. Decoupling the time channels in this way makes the inversion less sensitive to the specified uncertainties, but produces polarizabilities that are less smooth as a function of time.

Classification of Anomalies

At this stage in the process, we have feature vectors for each anomaly and need to decide which items should be excavated as potential UXO. For this demonstration, we employed library based techniques. Library based methods compare the recovered polarizabilities from a target to polarizabilities for a library of targets that may be found at the site. Anomalies are ranked according to the minimum misfit to the library items.

2.2 UXOLab Software

The methodologies for data processing, feature extraction, and statistical classification described above have been implemented within the UXOLab software environment, which was used for this demonstration. UXOLab is a Matlab based software package developed over a six year period at the UBC-GIF, principally through funding by the United States Army Corps of Engineers-Engineering Research and Development Center (USACE ERDC) (DAAD19-00-1-0120). Over the past seven years, BTG and UBC-GIF have considerably expanded the capabilities of the software.

2.3 Previous Testing of the Technology

Figure 1 provides a list of some of the previous tests conducted of the underlying data processing and interpretation methodology that will be used in this demonstration.

		1st Generation			Vehicle Mounted			Man Portable			Dynamic		
SITE	**PROJECT**	MAG	Geonics EM61	Geonics EM63	BUD	MetalMapper	TEMTADS 5x5	BUD-HH	MPV	TEMTADS 2x2	MetalMapper	MPV	TEMTADS 2x2
Former Lowry Bombing and Gunnery Range, CO	MM-0504	X	X	X									
Former Camp Sibert, AL	MM-0504	X	X	X	X								
Former Fort McClellan, AL	MM-0504			X									
San Luis Obispo, CA	MM-0504	X	X		X	X	X						
Former Camp Butner, NC	MR-1004		X			X	X						
Camp Beale, CA	MR-1004		X			X		X	X	X			
Pole Mountain, WY	MR-1159		X			X							
Spencer Range, TN	MR-1158,59					X	X		X	X	X	X	X
Camp Edwards, MMR, MA	MR-1226					X				X			
Camp George West, CO	MR-1228								X			X	
Camp Ellis, IL	MR-1226					X				X			
Ft. Rucker, AL	MR-1226					X							
New Boston, NH	**MR-1158,59**								X	X		X	
Southwest Proving Grounds, AL	**MR-1226**					X				X	X		X
Waikaloa, HI	**MR-1226**					X						X	

Figure 1: Previous Inversion/Classification Testing: A list of sites where classification has been applied and the types of sensor data that have been analyzed at each site. Green X's denote instances where industry geophysicists have processed datasets using UXOLab software after receiving training from BTG staff.

2.4 Advantages and Limitations of the Technology

The main advantage of the technology is a potential reduction in the number of non-hazardous items that need to be excavated, thus reducing the costs of UXO remediation. Advantages of UXOLab and the algorithms within the package include:

- All the functionality required to process raw geophysical data, detect anomalous regions, and perform geophysical inversion and classification.
- Algorithms for inverting magnetic and TEM data sets both separately and cooperatively using a number of different polarization tensor formulations.
- Extensive set of algorithms for rule-based and statistical classification algorithms.
- Configuration in a modular fashion, so that as new sensor technologies become available (e.g. new TEM systems with multi-component receivers etc), the inversion functionality will be immediately available to those new sensor systems.

The principal disadvantage is that UXOLab is written in Matlab and has not been configured for general use by contractors and non-specialists. However, as part of ESTCP MR-201226 we are presently working on transitioning our inversion algorithms to an API that will be generally accessible.

3.0 PERFORMANCE OBJECTIVES

The performance objectives for this demonstration are summarized in Table 1. Metrics specific to the MetalMapper and TEMTADS 2x2 datsets from Camp Ellis are summarized both in Table 2 and the ROC curves listed in Figure 2.

The first three analysis objectives refer to the classification part of the demonstration with the first two referring to the best results from each approach in a retrospective analysis and the third addressing how well each demonstrator is able to specify the correct threshold in advance. The final two objectives refer to the feature extraction part of the demonstration.

Table 1: Performance Objectives for the Camp Ellis demonstration.

Performance Objective	Metric	Data Required	Success Criteria
Maximize correct classification of TOI	Number of TOI retained	• Prioritized anomaly lists • Scoring reports from Institute for Defense Analysis (IDA)	Approach correctly classifies all TOI
Maximize correct classification of non-TOI	Number of false alarms eliminated	• Ranked anomaly lists • Scoring reports from IDA	Reduction of clutter digs by > 75% while retaining all TOI
Specification of no-dig threshold	Probability of correct classification of TOI and number of false alarms at demonstrator operating point	• Demonstrator -specified threshold • Scoring reports from IDA	Threshold specified by the demonstrator to achieve criteria above
Minimize number of anomalies that cannot be analyzed	Number of anomalies that must be classified as "Unable to Analyze"	• Demonstrator target parameters	Reliable target parameters can be estimated for > 95% of anomalies on each sensor's detection list.
Correct estimation of target parameters	Accuracy of estimated target parameters for seed items	• Demonstrator target parameters • Results of intrusive investigation	Polarizabilities -/+20% X, Y < 15 cm (1σ) Z < 10 cm (1σ)

Table 2: Performance Objectives for the Camp Ellis demonstration with sensor specific results for Metalmapper and TEMTADS 2x2.

Performance Objective	Metric	Success Criteria	Data Set	
			Metal-Mapper Cued	TEMTADS 2x2 Cued
Maximize correct classification of TOI	Number of TOI retained	Approach correctly classifies all TOI	**98.4%** of TOI (60 of 61) identified at stop dig point	**97.4%** of TOI (37 of 38) identified at stop dig point
Maximize correct classification of non-TOI	Number of false alarms eliminated	Reduction of clutter digs by > 75% while retaining all TOI	**55.8%** of non-TOI (525 of 941) dug at operating point	**50.8%** of non-TOI (495 of 974) dug at operating point
Specification of no-dig threshold	Probability of correct classification of TOI and number of false alarms at demonstrator operating point	Threshold specified by the demonstrator to achieve criteria above	P_{class} = 0.984 N_{fa} = 147 (15.6%)	P_{class} = 0.974 N_{fa} = 140 (14.4%)
Minimize number of anomalies that cannot be analyzed	Number of anomalies that must be classified as "Unable to Analyze"	Reliable target parameters can be estimated for > 95% of anomalies on each sensor's detection list.	99.8%	100%
Correct estimation of target parameters	Accuracy of estimated target parameters for seed items	Polarizabilities -/+20% X, Y < 15 cm (1σ) Z < 10 cm (1σ)	N(>20%)=0 N(<20%)=61 σ_x=0.06m σ_y=0.06m σ_z=0.03m	N(>20%)=1 N(<20%)=37 σ_x=NA σ_y=NA σ_z=0.06m

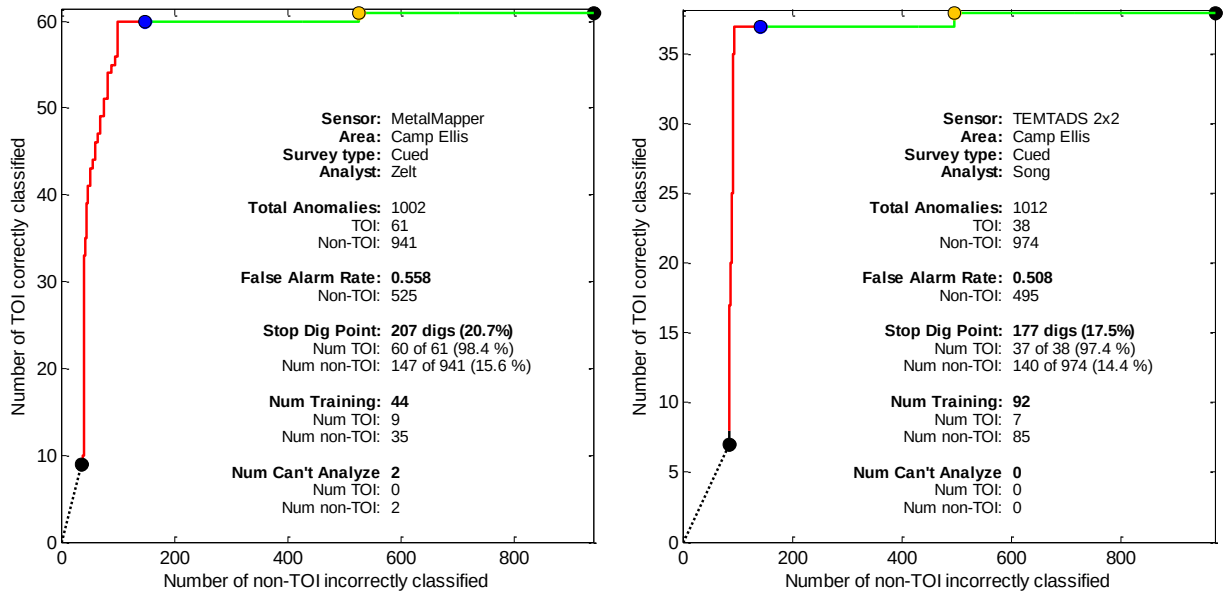

Figure 2: ROC curves and relevant classification statistics used to compute the metrics for the MetalMapper and TEMTADS 2x2 as listed in Table 2.

3.1 Objective: Detection of all TOI

This is one of the two primary measures of the effectiveness of the classification approach. By collecting high quality data and analyzing those data with advanced parameter estimation and classification algorithms we expect to be able to classify the targets with high efficiency. This objective concerns the component of the classification problem that involves correct classification of items-of-interest. The Quality of data should lead to a high probability of detecting the TOI at the site.

3.1.1 Metric

The metric for this objective is the percentage of seed items that are detected using the specified anomaly selection threshold.

3.1.2 Data Requirements

We will prepare an anomaly list. IDA personnel will score the detection probability of the seeded items.

3.1.3 Success Criteria

The objective will be considered to be met if 100% of the seeded items are detected within a halo of 60 cm.

3.2 Objective: Maximize Correct Classification of TOI

This is the second of the two primary measures of the effectiveness of the classification approach. By collecting high-quality data and analyzing those data with advanced parameter estimation and classification algorithms we expect to be able to classify the targets with high efficiency. This objective concerns the component of the classification problem that involves correct classification of TOI.

3.2.1 Metric

The metric for this objective is the number of items-of-interest on the master dig list that can be correctly classified as TOI by each classification approach.

3.2.2 Data Requirements

We will prepare a ranked anomaly list for the targets on the sensor anomaly list. IDA personnel will use their scoring algorithms to assess the results.

3.2.3 Success Criteria

The objective will be considered to be met if all of the TOI are correctly labeled as TOI on the ranked anomaly list.

3.3 Objective: Maximize Correct Classification of non-TOI

This is the second of the two primary measures of the effectiveness of the classification approach. By collecting high-quality data and analyzing those data with advanced parameter estimation and classification algorithms we expect to be able to classify the targets with high efficiency. This objective concerns the component of the classification problem that involves false alarm reduction.

3.3.1 Metric

The metric for this objective is the number of items on the sensor dig list that can be correctly classified as non-TOI by each classification approach.

3.3.2 Data Requirements

We will prepare a ranked anomaly list for the targets on the sensor anomaly list. IDA personnel will use their scoring algorithms to assess the results.

3.3.3 Success Criteria

The objective will be considered to be met if more than 75% of the non-TOI items can be correctly labeled as non-TOI while retaining all of the TOI on the dig list.

3.4 Objective: Specification of no-dig Threshold

In a retrospective analysis as will be performed in this demonstration, it is possible to tell the true classification capabilities of a classification procedure based solely on the ranked anomaly list submitted by each demonstrator. In a real-world scenario, all targets may not be dug so the success of the approach will depend on the ability of an analyst to accurately specify their dig/no-dig threshold.

3.4.1 Metric

The probability of correct classification of TOI, Pclass, and number of false alarms, Nfa, at the demonstrator-specified threshold are the metrics for this objective.

3.4.2 Data Requirements

We will prepare a ranked anomaly list with a dig/no-dig threshold indicated. IDA personnel will use their scoring algorithms to assess the results.

3.4.3 Success Criteria

The objective will be considered to be met if more than 75% of the non-TOI items can be correctly labeled as non-TOI while retaining all of the TOI at the demonstrator-specified threshold.

3.5 Objective: Minimize Number of Anomalies that Cannot be Analyzed

Anomalies for which reliable parameters cannot be estimated cannot be classified by the classifier. These anomalies must be placed in the dig category and reduce the effectiveness of the classification process.

3.5.1 Metric

The number of anomalies for which reliable parameters cannot be estimated is the metric for this objective.

3.5.2 Data Requirements

We will provide a list of all parameters as part of our results submission along with a list of those anomalies for which parameters could not be reliably estimated.

3.5.3 Success Criteria

The objective will be considered to be met if reliable parameters can be estimated for > 95% of the anomalies on each sensor anomaly list.

3.6 Objective: Correct Estimation of Target Parameters

This objective involves the accuracy of the target parameters that are estimated in the first phase of the analysis. Successful classification is only possible if the input features are internally consistent. The obvious way to satisfy this condition is to estimate the various target parameters accurately.

3.6.1 Metric

Accuracy of estimation of target parameters is the metric for this objective.

3.6.2 Data Requirements

In our demonstration report, we will compare their estimated parameters for the seed items to those expected.

3.6.3 Success Criteria

The objective will be considered to be met if the estimated polarizabilities are within ± 20%, the estimated X, Y locations are within 15 cm (1σ), and the estimated depths are within 10 cm (1σ).

4.0 SITE DESCRIPTION

Refer to the Program Office demonstration plan and the data collection demonstration plan prepared by ARCADIS for specifics regarding the site and data collection.

5.0 TEST DESIGN

Refer to the Program Office demonstration plan and the data collection demonstration plan prepared by ARCADIS for a description of the test design for the overall project.

6.0 DATA ANALYSIS AND RESULTS

In this section we describe our data analysis procedures in general. More detailed discussions specific to each of the two datasets summarized here are provided in Appendices A-D.

The Camp Ellis demonstration site involved the collection of both static, cued MetalMapper and TEMTADS 2x2 data, allowing a comparison of the relative performance of both sensors. Anomaly locations were selected using MetalMapper Dynamic data (Figure 3). MetalMapper cued data was acquired on the southern portion of the site, TEMTADS 2x2 was collected on the northern portion of the site and there were approximately 300 targets where cued measurements were made using both sensors in the central region of the demonstration as shown in Figure 4. A list of cued target picks was obtained from the Program Office for both the MetalMapper and TEMTADS 2x2 datasets. BTG proposed to process both MetalMapper and TEMTADS 2x2 cued datasets (with dynamic data being examined under the SERDP MR-2318 project). Processing the data from different sensors helps reinforce the sensor-independent nature of the processing algorithms and classification methodologies. It also provides an opportunity to compare the relative performance of the sensors. The workflow was similar for both datasets and is outlined in Figure 5. Classification was performed by a different BTG or UBC analyst for each dataset with a strict firewall maintained throughout the analyses. A comparison of classification performance of MetalMapper and TEMTADS 2x2 datasets from Camp Ellis is summarized in Table 3.

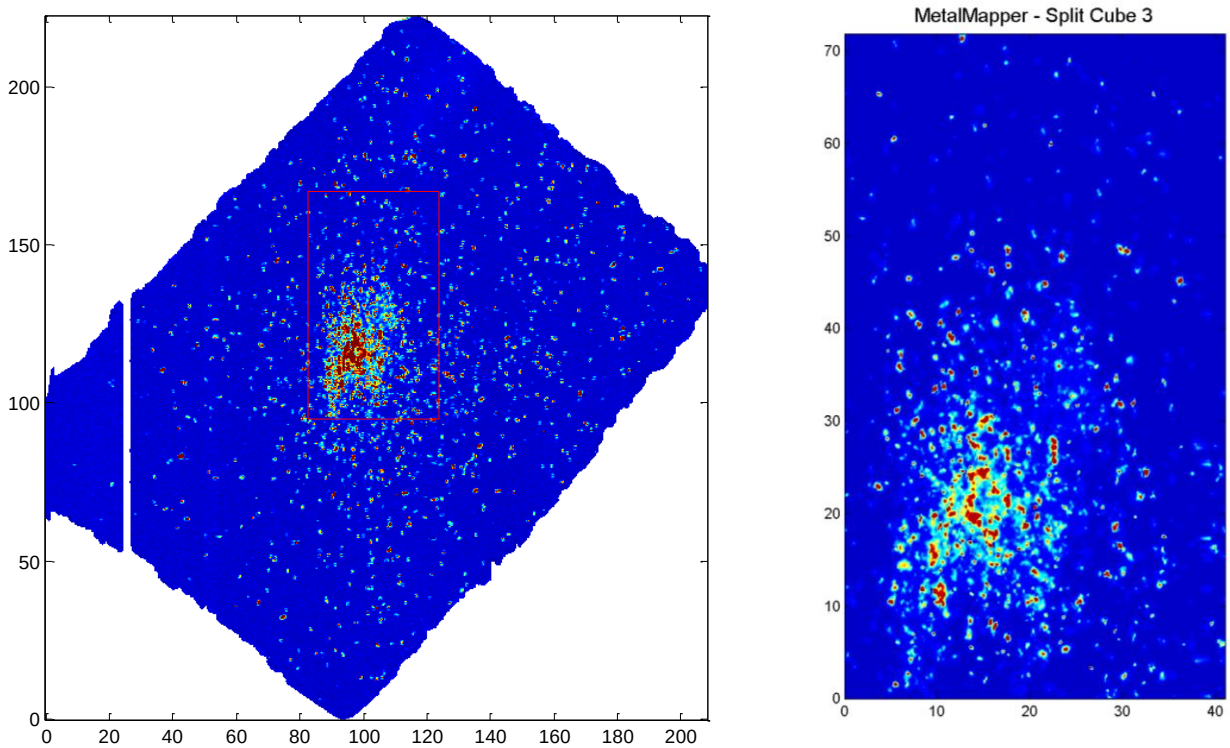

Figure 3: MetalMapper Dynamic data used to identify potential targets. The vertical component of the middle three cubes are gridded to form the image. An approximately 150 m x 200 m region of the former rocket, rifle grenade and hand grenade range was mapped with the MetalMapper. A high density region at the center of the map was also mapped by the TEMTADS 2x2 in a dynamic mode (red rectangle). On the right is a close-up of the region in the red rectangle.

(a) MetalMapper anomalies (b) TEMTADS 2x2 anomalies

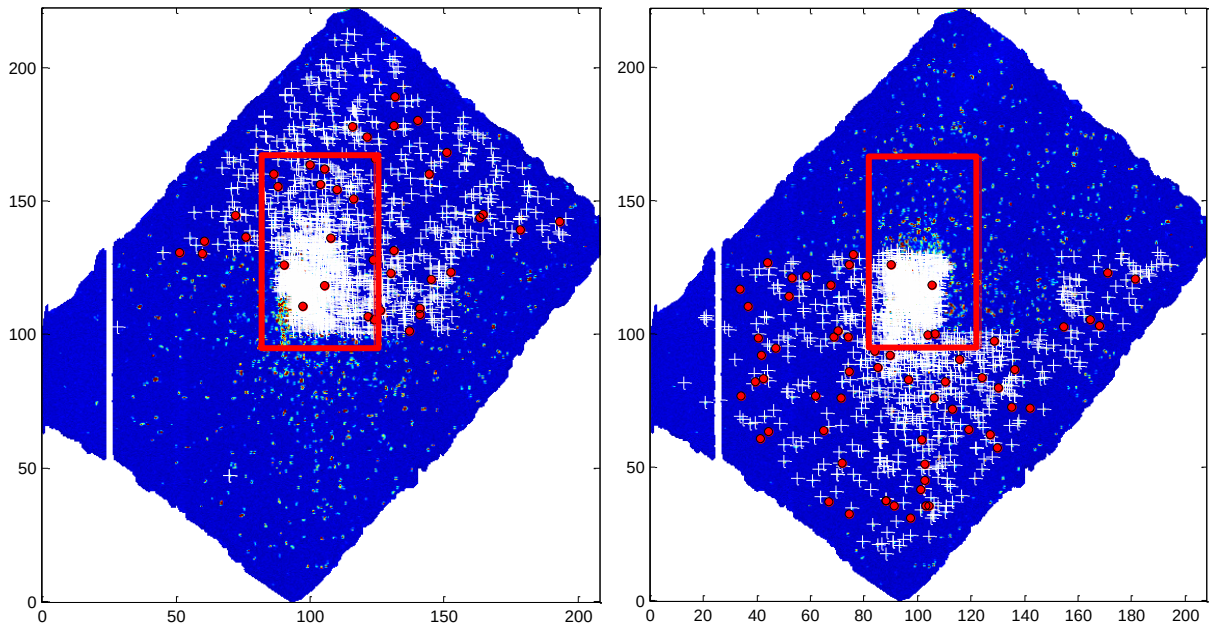

(c) Location of shared anomalies

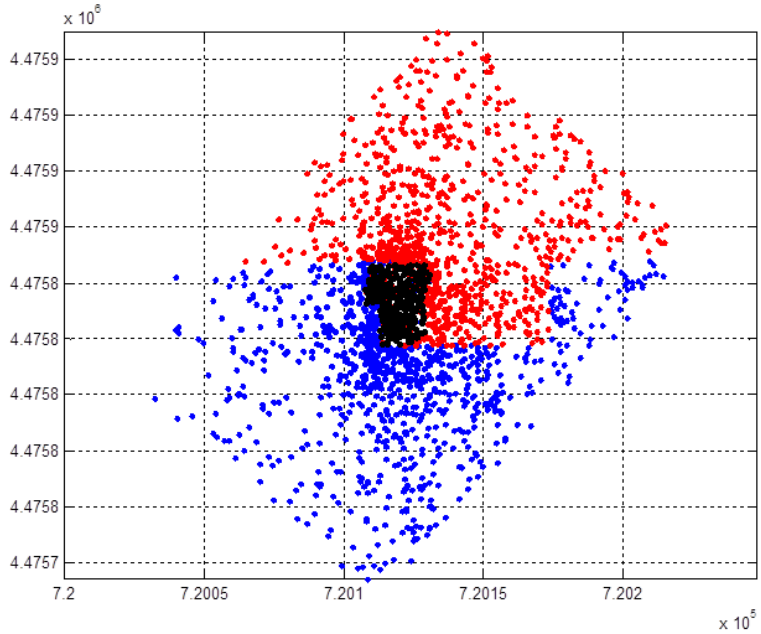

Figure 4: Camp Ellis cued data locations for MetalMapper and TEMTADS 2x2. In (a) and (b), the red dots represent targets of interest and non-TOI are represented by white '+' symbols. In (c), the red dots in the northern portion correspond to cued TEMTADS 2x2 measurements, blue dots in the south represent cued MetalMapper measurements while the black dots in the central region are locations where measurements were made with both sensors.

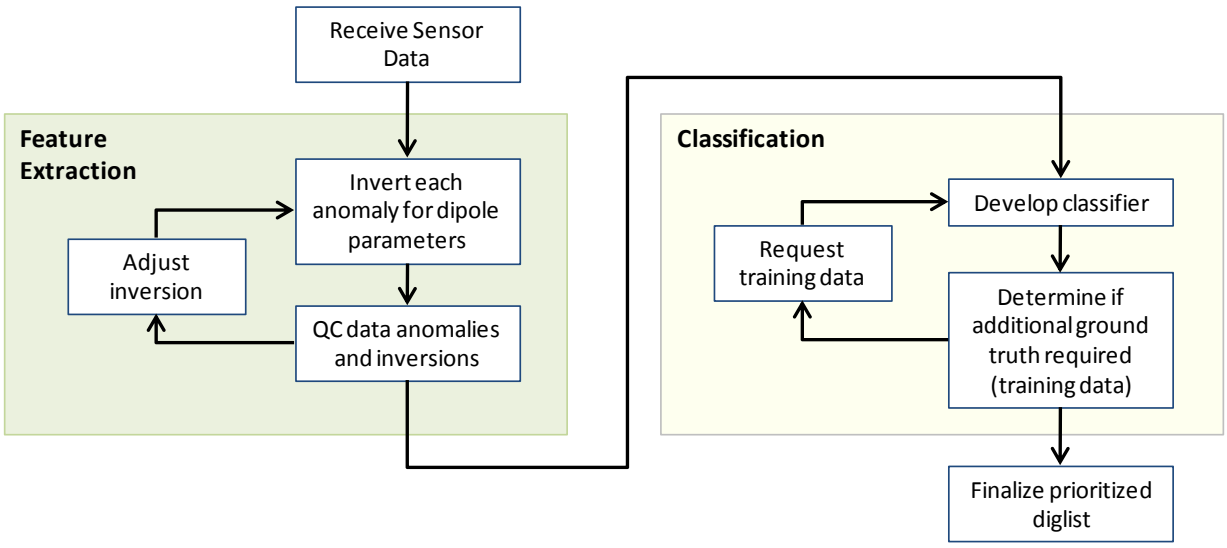

Figure 5: Overview of workflow applied to each dataset from Camp Ellis.

Table 3: Summary of classification performance for Camp Ellis MetalMapper and TEMTADS 2x2 datasets

	Instrument	**Metal Mapper**	**TEMTADS 2x2**
	Site	Camp Ellis	Camp Ellis
	Survey Type	Cued	Cued
	Analyst	Zelt	Song
Anomaly Statistics	Total Anomalies	1002	1012
	Num TOI	61	38
	Num Non-TOI	941	974
False Alarm Rate (FAR)	Percent of Non-TOI	0.558	0.508
	Num Non-Toi Dug	525	495
Stop Dig Point	Digs	207 (20.7%)	177 (17.5%)
	TOI Digs	60 (98.4 %)	37 (97.4 %)
	Non-TOI Digs	147 (15.6 %)	140 (14.4 %)
Training Data	Digs	44	92
	TOI	9	7
	Non-TOI	35	85
"Cant Analyze" anomalies	Digs	2	0
	TOI	0	0
	Non-TOI	2	0
Polarizability Percent Error	>20%	0	1
	<20%	61	37
Position Error	σ(Easting)	.06m	NA
	σ(Northing)	.06m	NA
	σ(depth)	.03m	0.06m

6.1 Cued MetalMapper Results

The MetalMapper consists of three orthogonal transmitters and seven multi-static receiver cubes (Figure 6). MetalMapper data were inverted using three inversions per anomaly, solving for (1) a single object (single object inversion: SOI); (2) two objects (2OI); and (3) three objects (3OI). BTG's *QCZilla* software was then used to review the one, two, and three dipole fits and identify the response most similar to a known TOI (and that produced a good fit to the data). In addition, BTG's custom training data selection tool, *TrainZilla* was used to explore feature space and automatically search for clusters of items with self-similar polarizabilities as shown in Figure 7. Training data requests typically focused on: (1) items whose polarizabilities exhibited UXO-like properties distinct from the items in our reference library; (2) items with polarizabilities similar to items in our reference library, but with degraded quality; and (3) one-off items. Figure 8 shows the location in decay-size feature space of all training requests. Particular attention was paid to an especially dense region of feature space (outlined by broken line in Figure 8). The polarizabilities of features within this large cluster are somewhat similar, but distinct from, those of the small ISO. We requested training for seven anomalies within this cluster. All of these turned out to be rocket weights (non-TOI). Training data were also requested for a number of items within the cluster of relatively fast decaying reference models for hand and rifle grenades obtained from test pit measurements. A new class of hand grenade (EL-373) and a 2.36" rocket were discovered and subsequently added to the reference library.

Figure 6: MetalMapper sensor collecting data at Camp Beale. Sensor consists of three orthogonal transmitters and seven multi-static receiver cubes.

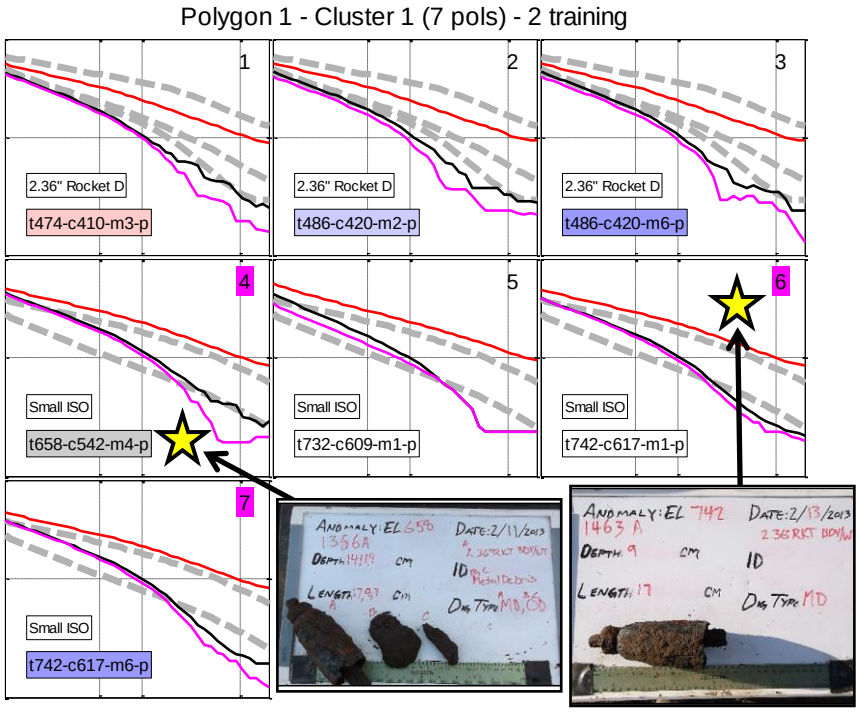

Figure 7: Polarizabilities for a cluster of self-similar polarizabilities identified with BTG's *TrainZilla* software. Colored lines are predicted polarizabilities. Broken grey lines are best fitting reference polarizabilities. Training data were requested for Anomalies EL-658 andEL-742 (stars); ground truth (photos) revealed that both of these anomalies are non-TOI (2.36" rocket bodies/weights (also metal debris in EL-658).

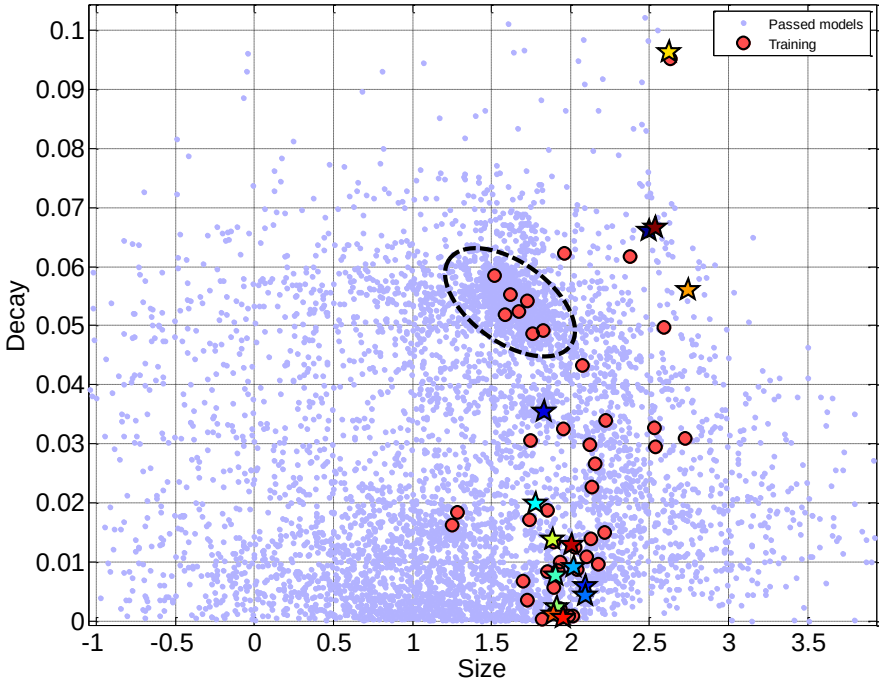

Figure 8: Decay versus size feature space plot showing passed models (blue dots) and the location of training data requests (red dots). Stars are library reference items.

The initial dig list comprised a single stage based on polarizability misfit to the best fitting library reference item for each model using matching on all three polarizabilities. The initial reference library comprised 14 items including several variants of the same ordnance class (unique ordnance classes included 2.36-inch rocket, small ISO, steel rifle grenade, aluminum rifle grenade, and hand grenade). The stop dig point was set at dig number 154. This stage 1 dig list missed two QC seeds. One of the missed seeds (EL-132 rifle grenade) was a slight variant of the library rifle grenade with an offset in the primary polarizability relative to the best matching item in the reference library. Polarizabilities for EL-132 were added to the reference library to ensure that the seed and similar items were dug. The second missed seed was a 2.36-inch rocket (EL-1522). This particular seed is lacking most of the head and all of the tail assembly and therefore more closely resembles a rocket motor (considered non-TOI at the Camp Ellis site). However, because this particular seed was considered TOI, its polarizabilities for EL-1522 were added to the reference library. After adding polarizabilities for the two missed seeds to the reference library, several more digs were required and the stop dig point for the stage 2 dig list was set at dig 206. After receiving stage 2 ground truth, items with the best fitting two or three polarizabilities (relative to library polarizabilities) beyond the stage 2 stop dig point were identified and manually moved up the dig list. This resulted in thirteen additional items being dug. One additional item was also classified as "cannot analyze" to arrive at the final stage 3 dig list with a stop dig point of dig 220.

The final dig list (see ROC curve in Figure 9) missed one TOI: (1) EL-941, a rifle grenade at 19cm depth. Polarizabilities and ground truth photo for EL-941 are shown in Figure 10. The best fitting reference item ("Steel RG D") was based on EL-132, which was one of the two missed QC seeds from stage 1. In creating the reference polarizabilities for the missed QC seed, multi-object inversion models were chosen as they provided the best fit to a reference item created from high quality test pit measurements. In this case, EL-941 is a much better match to the single object inversion result for EL-132 and had the SOI model been used as a reference, EL-941 would have occurred much earlier in the dig list and would likely have been dug. Another factor making EL-941 an especially difficult target is evident in comparing the photos of EL-941 and EL-132 shown in Figure 10. Note that EL-941 is not intact compared with EL-132 and is missing part of the head and the tail fins.

Additional details on the MetalMapper classification approach can be found in the Decision Memo prepared by the MetalMapper analyst which is included in Appendix A in its entirety

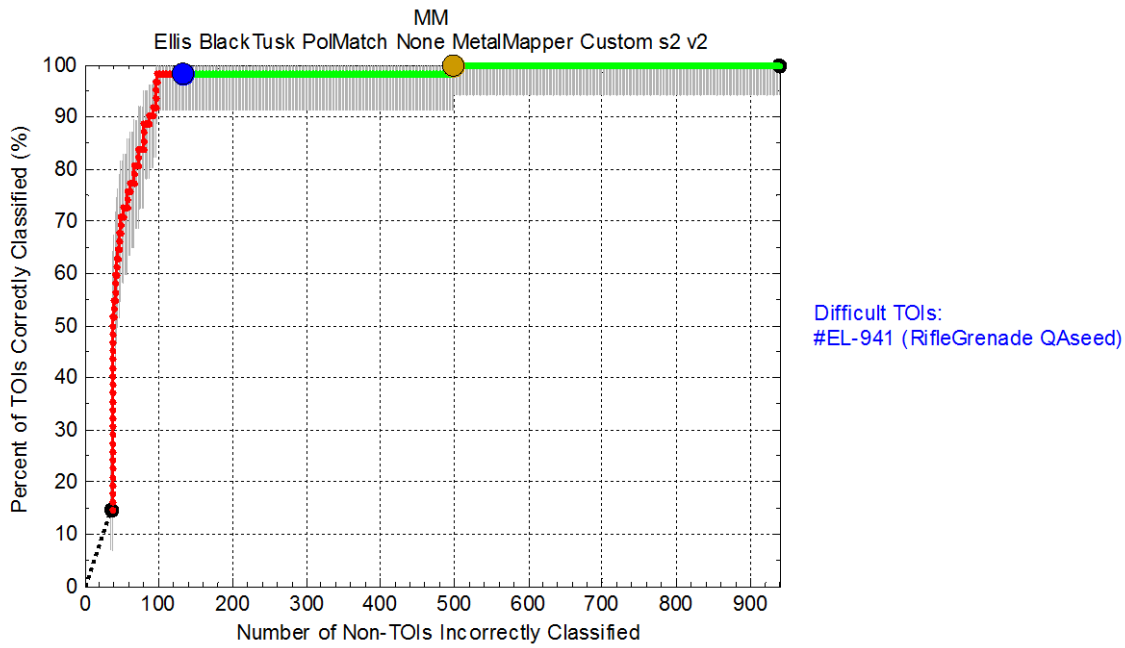

Figure 9: Final ROC curve for cued MetalMapper data from Camp Ellis.

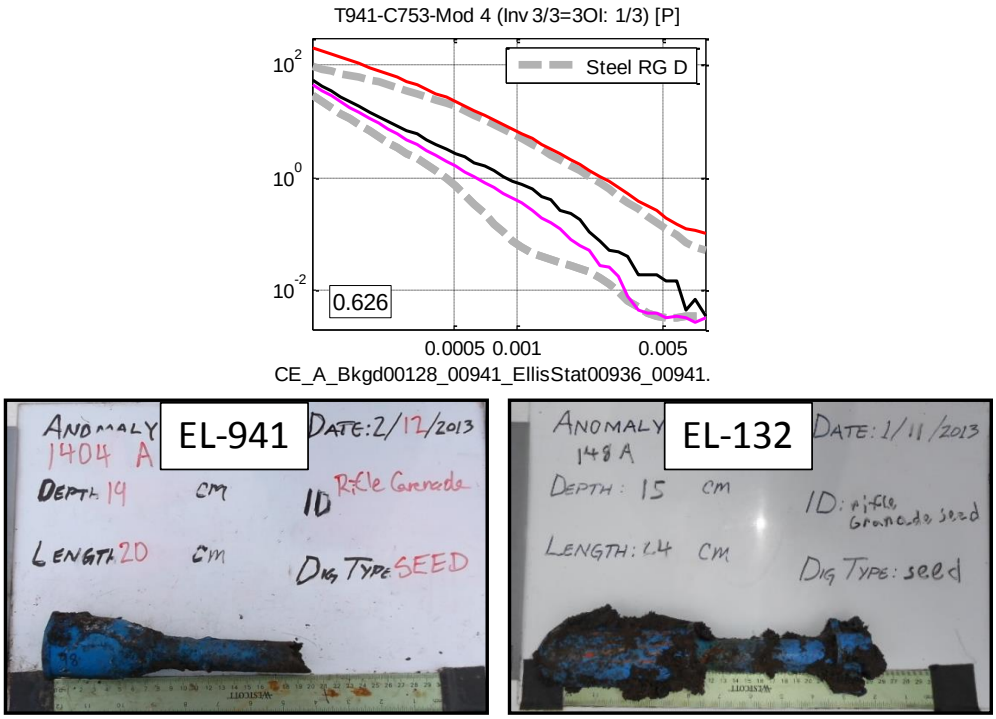

Figure 10: Top: polarizabilities for missed TOI EL-941 (colored lines), a rifle grenade at 19 cm depth, and the best fitting rifle grenade reference polarizabilities ("Steel RG D", which were based on EL-132: broken grey lines). Bottom Left: ground truth photo for El-941. Note that the rifle grenade is not intact. Bottom Right: ground truth photo for EL-132. Note that this rifle grenade is intact.

Figure 11: The TEMTADS 2x2 instrument being operated at the Former Spencer Artillery Range

6.2 Cued TEMTADS 2x2

The TEMTADS 2x2 sensor consists of a 2x2 grid of transmitters, with a three-component receiver at the center of each receiver (Figure 11). Inversions were run on TEMTADS 2x2 data using single, two, and three object inversions. Classification was performed using a library matching method based on how well target polarizabilities matched a set of TOI library polarizabilities. The library matching involved four main stages:

1) build a polarizability library initially based on test pit and IVS data,
2) assess the match of cued target polarizabilities to the library,
3) request training data, and
4) produce a ranked anomaly list.

Training data requests typically focused on: (1) items whose polarizabilities exhibited UXO-like properties distinct from the items in our reference library, (2) items with polarizabilities similar to items in our reference library, but with degraded quality, and (3) one-off items.

Figure 12 shows examples of targets with axis-symmetric polarizabilities that were not matched to items in the reference library. Training data requests for these items indicated that these items were non-TOI (munitions debris and rocket motors).

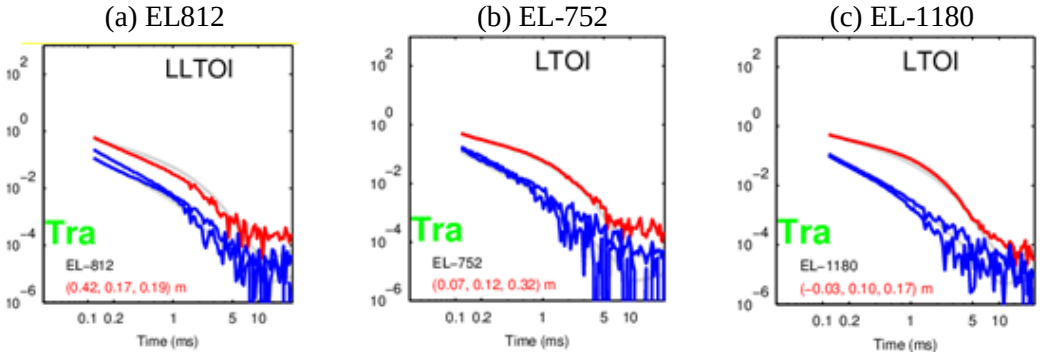

Figure 12: Selected training data requests all of which were revealed to be non-TOI including: (a) munitions debris (EL-812) and (b, c) 2.36" rocket motors (EL-752, EL-1180).

The initial dig list comprised a single stage based on polarizability misfit to the best fitting library reference item for each model using all three polarizabilities. The initial reference library contained 14 items comprised of seven ordnance classes with several variants for some of the ordnance classes (e.g. hand/rifle grenades). The stop dig point was set at dig number 165. This stage 1 dig list missed one QC seed, a hand grenade (EL-143). Ground truth for EL-143 revealed that 3 items were present: a TOI hand grenade as well as non-TOI 2.36" rocket and non-TOI 2.36" rocket weight. In training data requests, EL-143 was grouped with 8 targets with similar polarizabilities. Three of those eight items (shown in Figure 12) were selected for training data. When all three were reported to be non-TOI, the remaining five items (including EL-143) were also classified as non-TOI. With the feedback from the missed QC seed and training requests suggesting potentially difficult to identify TOIs, it was decided that whenever there was at least a pair of suspected anomalies, they should be dug or requested for training to ensure the maximum probability of digging all TOI anomalies. 16 additional targets were dug in stages 3 and 4 all of which were confirmed to be non-TOI; the final dig list was submitted with a stop dig point of 181.

The final dig list (ROC curve results shown in Figure 13) missed one QC seed, a rifle grenade (anomaly EL-941). Anomaly EL-941 best matched a reference library item that had been identified as a non-TOI rocket motor through training requests. Additional details on the TEMTADS 2x2 classification approach can be found in the Decision Memo prepared by the TEMTADS 2x2 analyst which is included in Appendix D in its entirety.

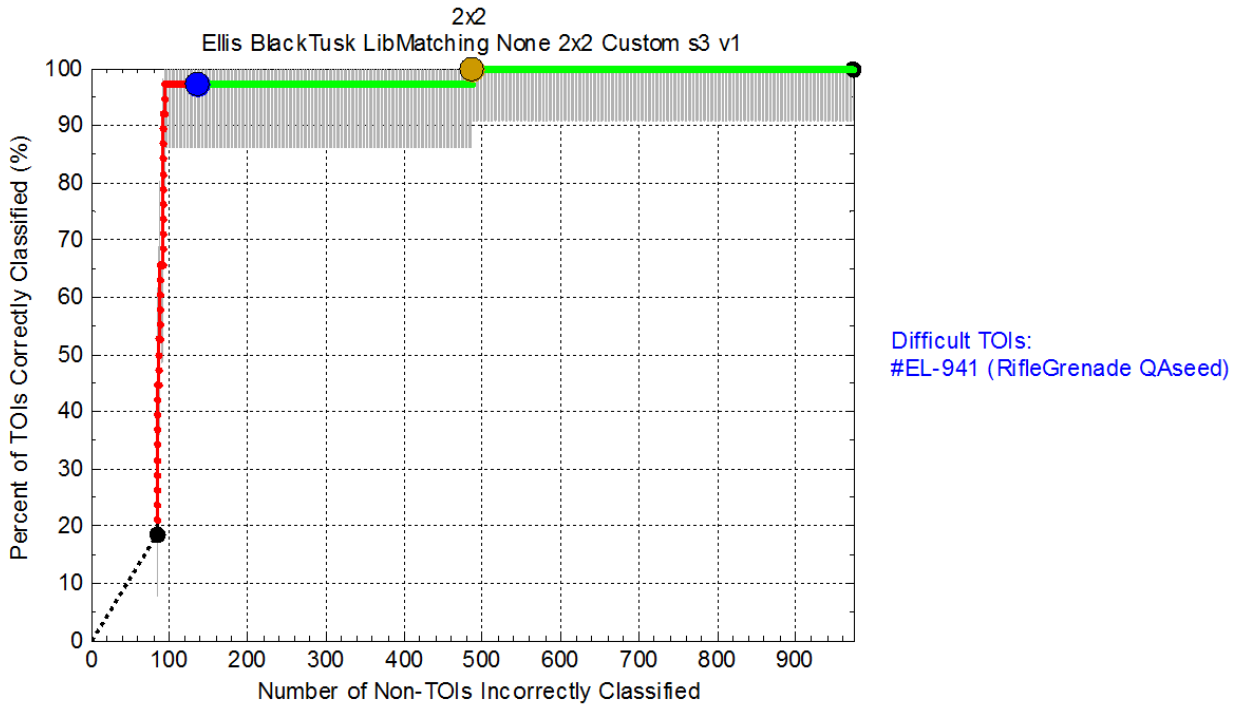

Figure 13: Final ROC curve for cued TEMTADS 2x2 data from Camp Ellis.

7.0 MANAGEMENT AND STAFFING

A flow chart showing the managerial hierarchy and the relationship between the principal investigator (PI) and other personnel is shown in Figure 14.

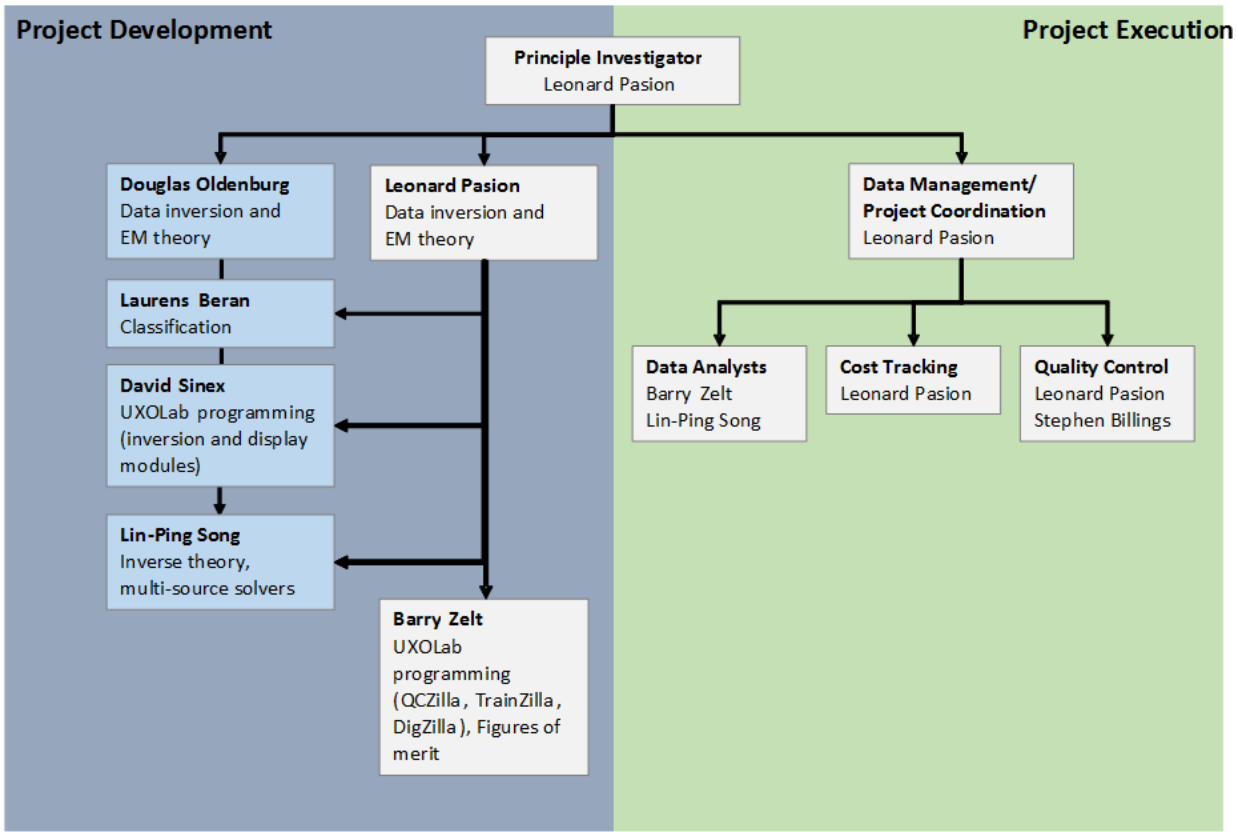

Figure 14: Project management hierarchy showing BTG personnel in blue and UBC-GIF personnel in green. The hierarchy is split between the development and execution components.

8.0 REFERENCES

T. Bell, B. Barrow, J. Miller, and D. Keiswetter. Time and frequency domain electromagnetic induction signatures of unexploded ordnance. Subsurface Sensing Technologies and Applications,2:153-175, 2001.

ESTCP. 2010 ESTCP demonstration study, former Camp Butner. Technical report, 2010.

X. Liao and L. Carin. Migratory logistic regression for learning concept drift between two data sets with application to UXO sensing. IEEE Trans. Geosci. Remote Sensing, 47:1454 -1466, 2009.

L. R. Pasion, S. D. Billings, D. W. Oldenburg, and S.Walker. Application of a library-based method to time domain electromagnetic data for the identification of unexploded ordnance. Journal of Applied Geophysics, 61:279-291, 2007.

F. Shubitidze, K. O'Neill, S. A. Haider, K. Sun, and K. D. Paulsen. Application of the Method of Auxiliary Sources to the Wide-Band Electromagnetic Induction Problem. IEEE Trans. Geosci. Remote Sensing, 40:928-942, 2002.

S. L. Tantum, Y. Li, and L. M. Collins. Bayesian mitigation of sensor position errors to improve unexploded ordnance detection. IEEE Geosci. Remote Sensing Letters, 5:103{107, 2008.

G. F. West and J. C. Macnae. Electromagnetic methods in applied geophysics, chapter Physics of the electromagnetic exploration method, pages 5-45. SEG, 1991.

9.0 APPENDICES

Appendix A: MetalMapper Feature Extraction and Classification

MetalMapper Cued Feature extraction (open area)

MetalMapper cued data for all anomalies were received as a set of raw TEM files and a set of CSV files with background corrections applied. Our analyses used the background-corrected data. The data were inverted in UXOLab using a sequential inversion approach to estimate target location, depth and primary polarizabilities. Instrument height above the ground was assumed to be 10 cm. Noise standard deviation estimates were not available, so a constant noise value of 1 over all time channels was used. Target location was constrained to lie between ±0.7 m in both X and Y directions relative to the picked location. Target depth was constrained to lie between –1.2 and 0 m. The initial optimization for target location identified up to five starting models to input into the subsequent estimation of polarizabilities. We performed three inversions per anomaly, solving for (1) a single object (single object inversion: SOI); (2) two objects (2OI); and (3) three objects (3OI).

Analysis of the data, including visual QC of data and model parameters, selection of training data, and dig list creation, was performed using the UXOLab software suite. Visual QC of the data was performed using the UXOLab module *QCZilla*, which provides a thorough overview of the observed and predicted data, predicted model parameters, and measures of data/model quality. Display of the gridded EM61 data at each anomaly provides a useful indicator of the anomaly size and strength. Predicted polarizabilities were compared to reference polarizabilities for various ordnance items initially derived from IVS and test pit measurements. The Camp Ellis IVS contained three ordnance items: hand grenade, small ISO and partial steel rifle grenade. In addition, measurements were taken in a test pit using a 2.36" rocket, aluminum rifle grenade, steel rifle grenade, hand grenade and small ISO, all at various depths and orientations. As the analysis proceeded, the library of reference items was augmented with additional items based on ground truth obtained through training data requests and partial ground truth. Each item in the ordnance reference library was assigned a size (diameter) in mm. Each item classified as "likely TOI" in the submitted dig list was assigned a size based on the ordnance item in the reference library with the best matching primary polarizability (L1).

During data/model QC the primary objectives were to (1) flag high-likelihood TOI anomalies; and (2) fail bad models and inversions. Anomalies flagged as high-likelihood TOI were monitored during the dig list creation phase to ensure they were being dug, ideally early in the dig list. Models and inversions were considered to be bad when the inversion failed (i.e., the data misfits are large), or when the recovered model location(s) were on, or near, an inversion boundary. Bad models and inversions were identified in a semi-automated manner. E.g., models would be sorted by different measures of polarizability/data quality and the visual QC process would focus on the models with the poorest quality.

With multi-object inversions it is not uncommon that one of the models is unrealistic (e.g., deep, large in magnitude, sometimes located on or near a horizontal inversion boundary) yet provides the best fit to the reference polarizabilities (e.g., Figure 15). In all of these cases the model was flagged as failed. Models flagged as failed were not used in the classification process. Anomalies with all models from all inversions failed were classified as "cannot extract reliable parameters"; these anomalies were dug. For a given anomaly, if more than one model was passed the classification procedure will consider all passed models and effectively use the one that is "best" based on the classification metric.

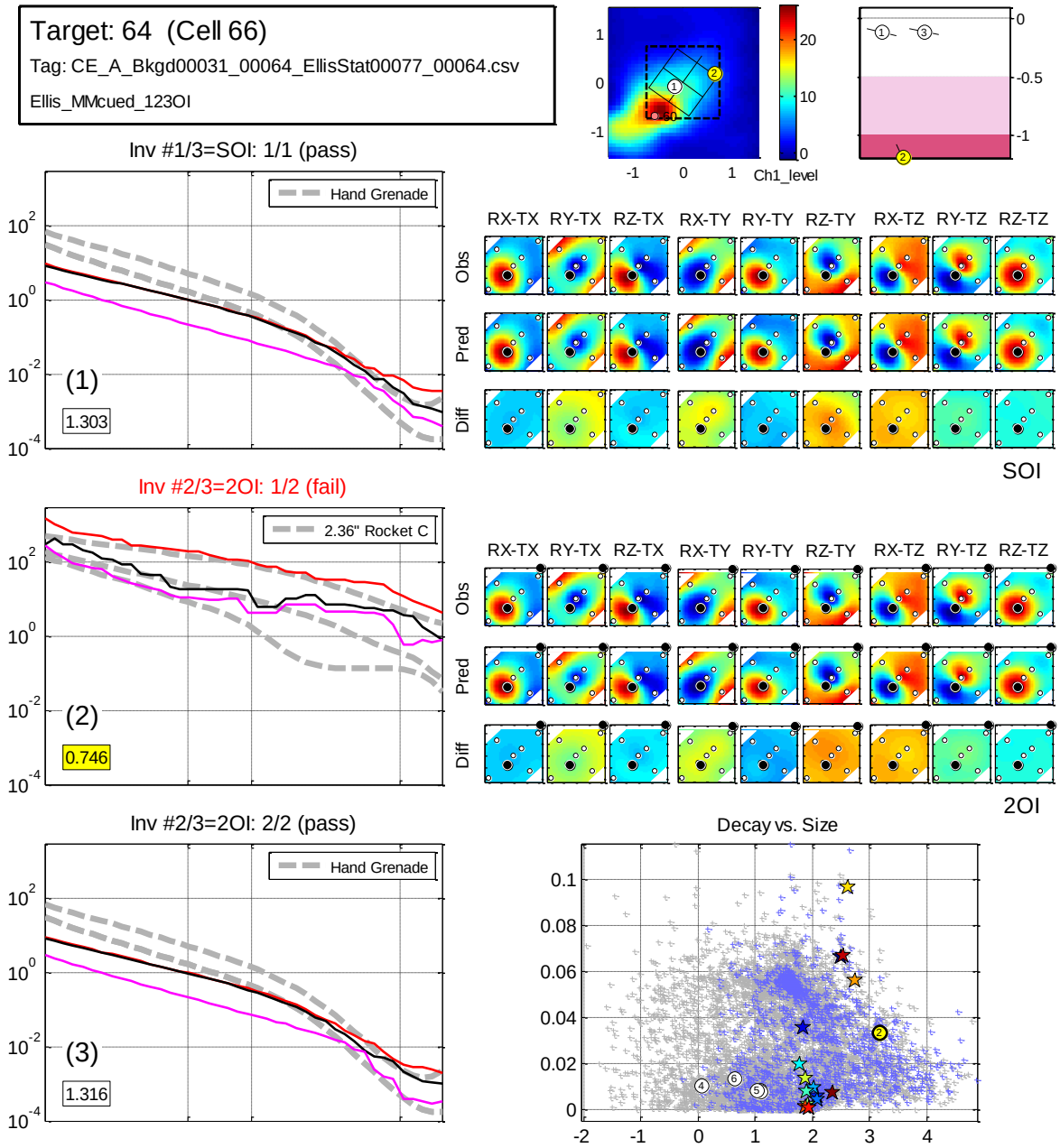

Figure 15: Example of an unrealistic 2OI model (anomaly 1250; frag). The first model of the 2OI (model 2) provides the best fit (i.e., minimum misfit) to the reference polarizabilities (misfit = 0.746), but the predicted depth of 1.2m and location at the edge of the instrument (i.e., at the vertical and horizontal inversion boundaries), and high amplitude and jittery appearance of the polarizabilities are classic signs that this model is an artifact of the multi-object inversion process. Accordingly, this model was failed during QC. Polarizabilities for SOI and 2OI are shown at left. Modeled target locations (X-Y and Z) are shown at the top right (gridded EM61 data is displayed behind the X-Y plot). Gridded observed, predicted and residual data for SOI and 2OI are shown below location maps. Decay versus size feature plot is shown in bottom right. Dots are test data; stars are reference items. Numbered circles are models for this anomaly.

Training data selection

Figure 16 shows the distribution of passed models in decay versus size feature space.

Our analysis method is based on polarizability matching with respect to ordnance items in a reference library. For this approach to be successful it is important to determine the types of ordnance present at the site. During visual QC the analyst keeps track of suspicious, UXO-like items (i.e., items with modeled polarizabilities possessing UXO-like properties). Training data for some of these, particularly those with polarizabilities different from the items in the reference library, would be requested. In addition, we used our custom training data selection tool, *TrainZilla*, to explore feature space and automatically search for clusters of items with self-similar polarizabilities. In *TrainZilla*, the user selects a region in feature space by drawing a polygon, and the program automatically identify clusters of self-similar feature vectors by computing a misfit matrix **M** with elements

$$M_{jk} = \sum_{i=1}^{N} (L^{j}{}_{total}(t_i) - L^{k}{}_{total}(t_i))^2$$

where L^{j}_{total} is the log-transformed total polarizability for the jth feature vector. Feature vectors with mutual misfit less than a user-specified threshold define a cluster in polarizability space. This analysis helps to identify clusters that may not be readily evident in decay-size feature space: e.g., targets with consistent polarizabilities that may be hidden in the "cloud" of non-TOI features. A basic example of the use of *TrainZilla* is shown in Figure 17 and Figure 18.

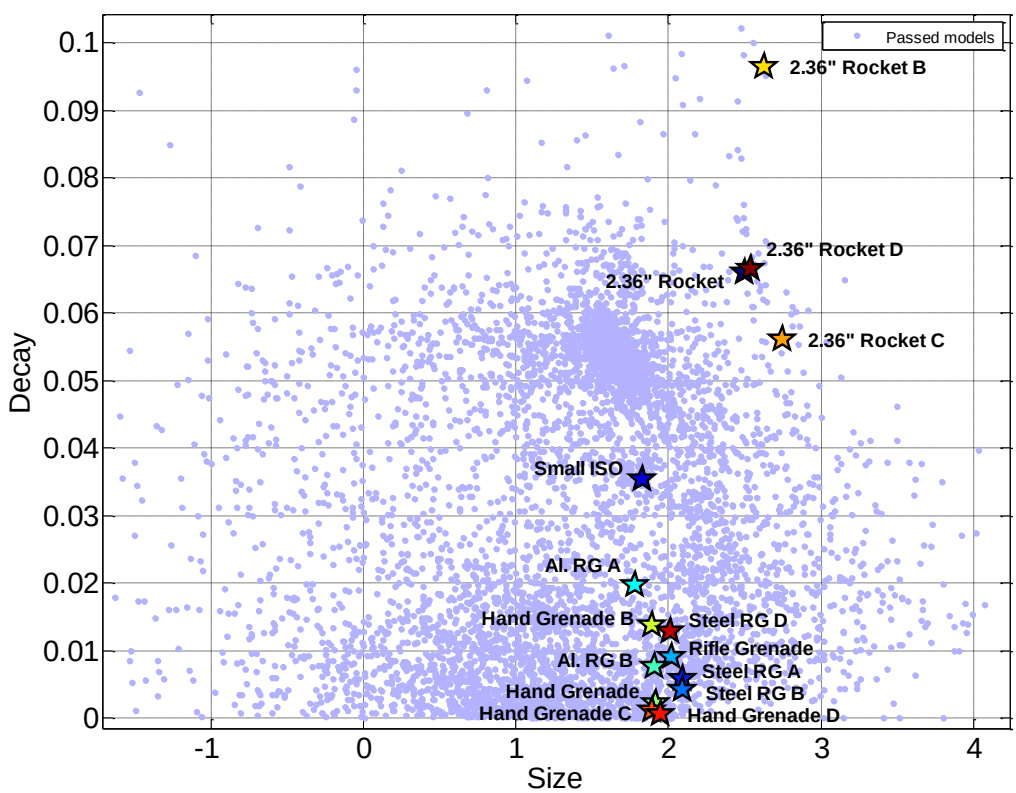

Figure 16: Distribution of passed models in decay(t1,t29) versus size(t1) feature space, where size(t1) is the total polarizability measured at the first time channel (t1=0.106ms), and decay(t1,t29) is size(t1)/size(t29) where t29=2.006ms. Some outliers are not shown. Labeled stars represent ordnance library reference items.

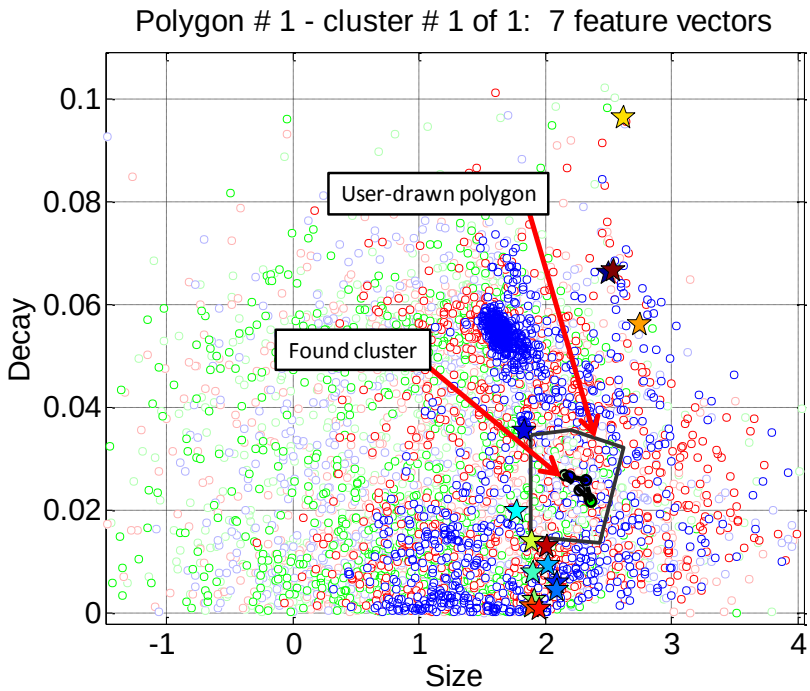

Figure 17: Example of use of the training data selection tool (*TrainZilla*). A polygon (solid black line) is drawn in feature space. Clusters of items with self-similar polarizabilities are automatically found based on the specified cluster search parameters. In this case a cluster comprising 7 features is visible (solid feature symbols encompassed by broken line). Polarizabilities for this cluster are shown in Figure 18.

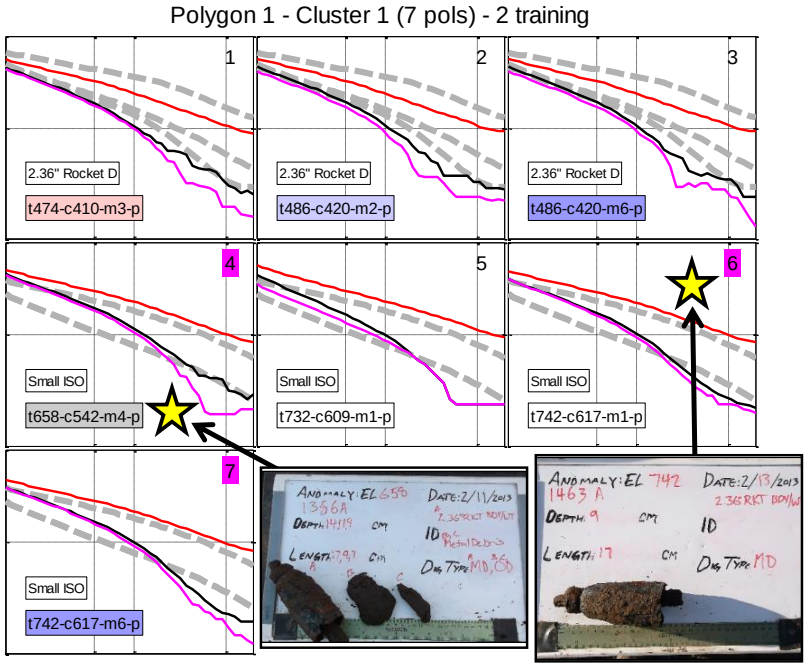

Figure 18: Polarizabilities for the cluster shown in Figure 17. Colored lines are predicted polarizabilities. Broken grey lines are best fitting reference polarizabilities. Training data were requested for Anomalies EL-658 andEL-742 (stars); ground truth (photos) revealed that both of these anomalies are non-TOI (2.36" rocket bodies/weights (also metal debris in EL-658).

Our training data requests typically focused on: (1) items whose polarizabilities exhibited UXO-like properties distinct from those of items in our reference library (such as the example in Figure 17 and Figure 18; (2) items with polarizabilities similar to items in our reference library, but with degraded quality; and (3) one-off items. Figure 19 shows the location in decay-size feature space of all training requests. We paid particular attention to a particularly dense region of feature space (outlined by broken line in Figure 19). The polarizabilities of features within this large cluster are somewhat similar, but distinct from, those of the small ISO. We requested training for seven anomalies within this cluster. All of these turned out to be rocket weights (non-TOI).

In our initial training request for 35 items, only three were TOI. One of these (EL-645) was subsequently removed from the anomaly list. The other two were a new class of hand grenade (EL-373) and a 2.36" rocket. We requested training for eight additional anomalies in three subsequent requests. Five of these were TOI, but no new classes of TOI were discovered.

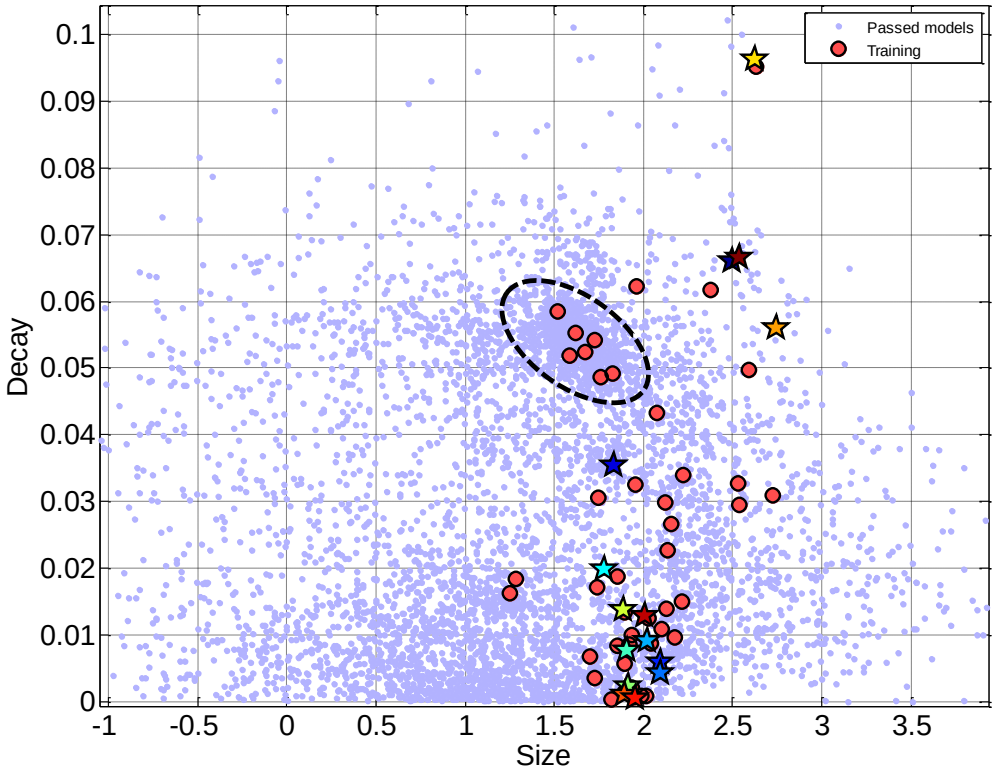

Figure 19: Decay versus size feature space plot showing passed models (blue dots) and the location of training data requests (red dots). Stars are library reference items. Broken black line outlines a region of high feature density.

Classification method

Our dig lists were developed using our visual classification software *DigZilla* (Figure 20), which is fully integrated with other elements of the UXOLab software suite. *DigZilla* allows for the creation of multi-stage dig lists with minimal effort, and supports a number of classifiers.

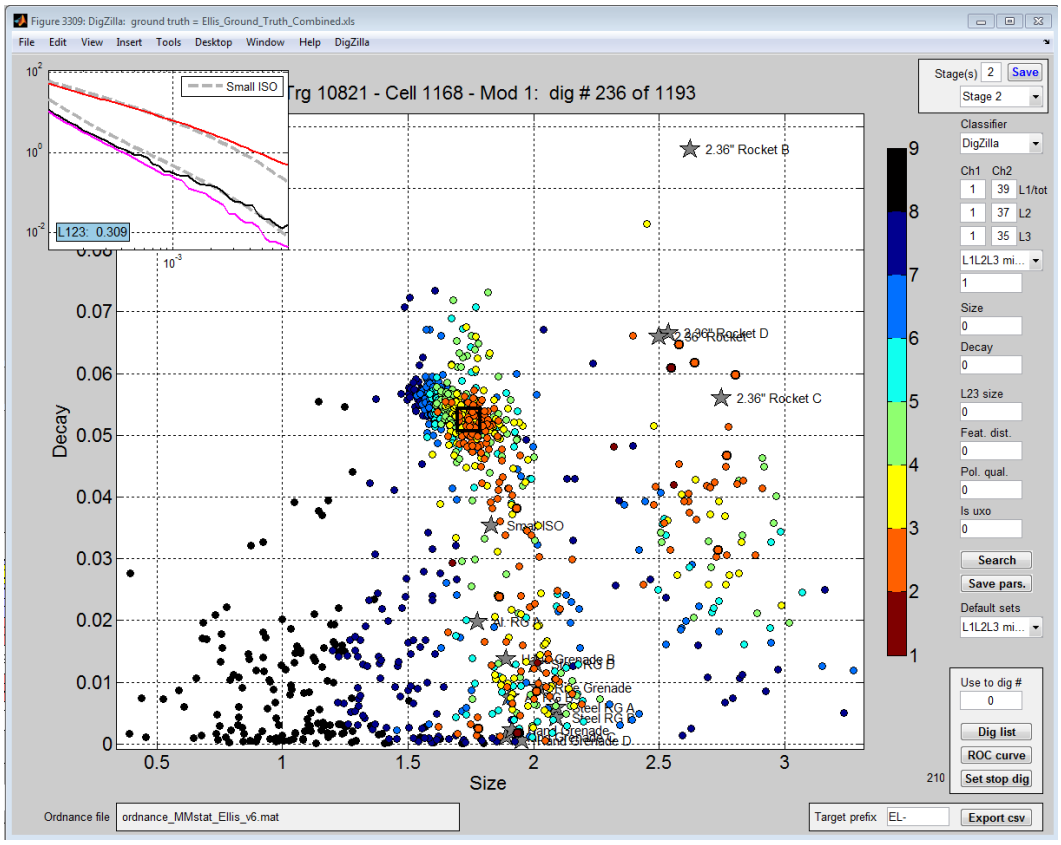

Figure 20: Screen shot of the UXOLab *DigZilla* graphical user interface. Features in the decay versus size feature plot are color coded according to dig list order.

Our initial (stage 1) dig list comprised a single stage based on polarizability misfit (to best fitting library reference item for each model) using all three polarizabilities. For this stage, and all subsequent stages, misfits for the primary, secondary and tertiary polarizability were calculated between the first time channel and channels 39 (5.77 ms), 37 (4.67 ms) and 35 (3.78 ms), respectively. The maximum time channels to use were determined automatically using a measure of average polarizability reliability. Our initial ordnance library comprised 14 items, several of which were variants of the same ordnance class. The distinct ordnance classes in this library were: 2.36" rocket, small ISO, steel rifle grenade, aluminum rifle grenade and hand grenade. The stop dig point for this list was dig number 154.

Our stage 1 dig list missed two QC seeds. Because of this we were required to submit a Failure Analysis Memo, which is presented below in its entirety.

Failure Analysis Memo

Site: Camp Ellis
Analyst: Black Tusk Geophysics
Data: MM Cued
Date: July 31, 2013

Our stage 1 dig list missed two QC seeds (Table 4).

Table 4. List of missed QC seeds.

Anomaly	Depth (cm)	Identification	Dig Number
EL-132	15	Seed (RIFLE GRENADE)	410
EL-1522	15	SEED (2.36" RKT)	883

a. Analysis of the factors that resulted in the misclassification of each missed seed

EL-132 (rifle grenade at 15 cm depth)

Our classification method is based primarily on matching polarizabilities with items in an ordnance reference library. Polarizabilities for EL-132 are shown in Figure 21. The best fitting item in our reference library was the steel RG (taken from test pit measurements). The calculated misfit value (based on the differences of all three polarizabilities (primary, secondary, tertiary) is 0.412. In comparison, the stop dig point on our stage 1 dig list corresponded to a misfit value of ~0.30. The relatively large misfit for EL-132 is primarily due to the offset in the primary polarizability. To ensure that our classification approach finds similar items, we will add a set of polarizabilities to our ordnance reference library based on the EL-132 polarizabilities.

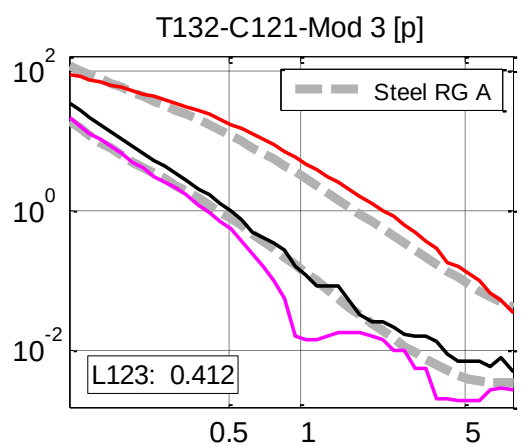

Figure 21: Polarizabilities for EL-132 (rifle grenade; red, black and magenta lines) relative to polarizabilities for the steel rifle grenade reference item from test pit measurements (broken grey lines).

EL-1522 (2.36" rocket at 15 cm depth)

The polarizabilities for EL-1522 (Figure 22a) are significantly different from the 2.36" rocket reference polarizabilities derived from test pit measurements (misfit value = 0.658). The ground truth photo shows that, in comparison to a mostly intact 2.36" rocket (e.g., EL-1719) , the seed used at EL-1522 is missing most of the head and all of the tail assembly (or vice versa; Figure 22b-c). This difference explains the difference between recovered and reference polarizabilities. The object at EL-1522 is virtually nothing more than a rocket motor (which is considered a non-TOI for this site). The similarity in the physical shape and recovered polarizabilities for the partial 2.36" rocket at EL-1522 and a rocket motor, is apparent in Figure 23. Unfortunately, because the seed at EL-1522 is considered a TOI we must dig items with similar responses. This implies that we will now be digging a lot of objects that look very much like rocket motors. More than likely, most, if not all, of these will turn out to be rocket motors.

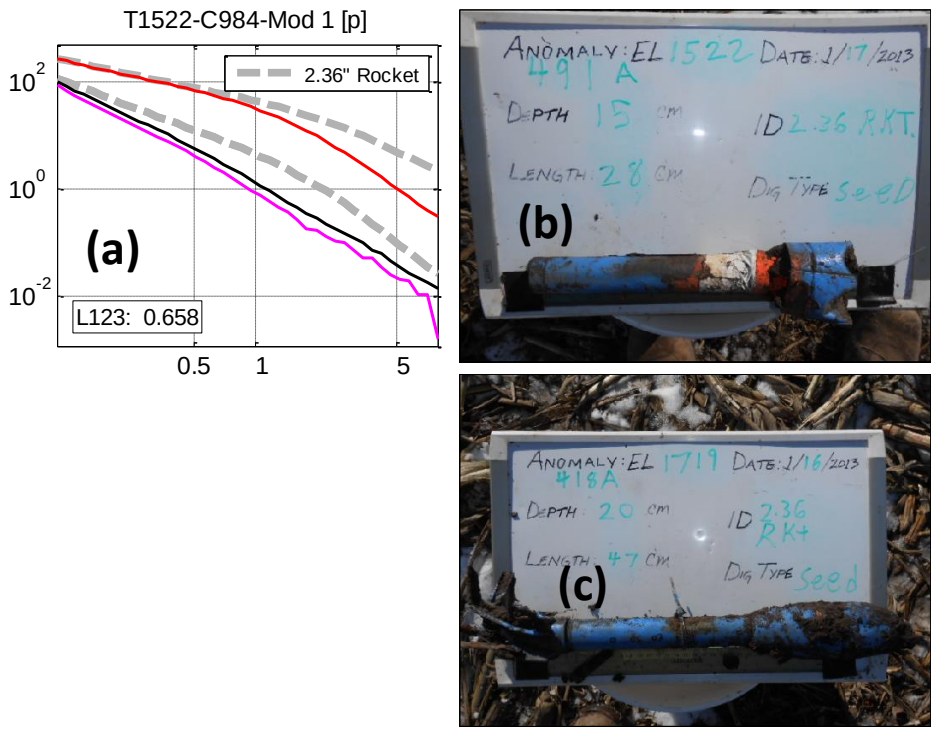

Figure 22: (a) Polarizabilities for EL-1522 (2.36" rocket) relative to polarizabilities for the 2.36" rocket reference item from test pit measurements. (b) Ground truth photo for EL-1522. (c) Ground truth photo for EL-1719.

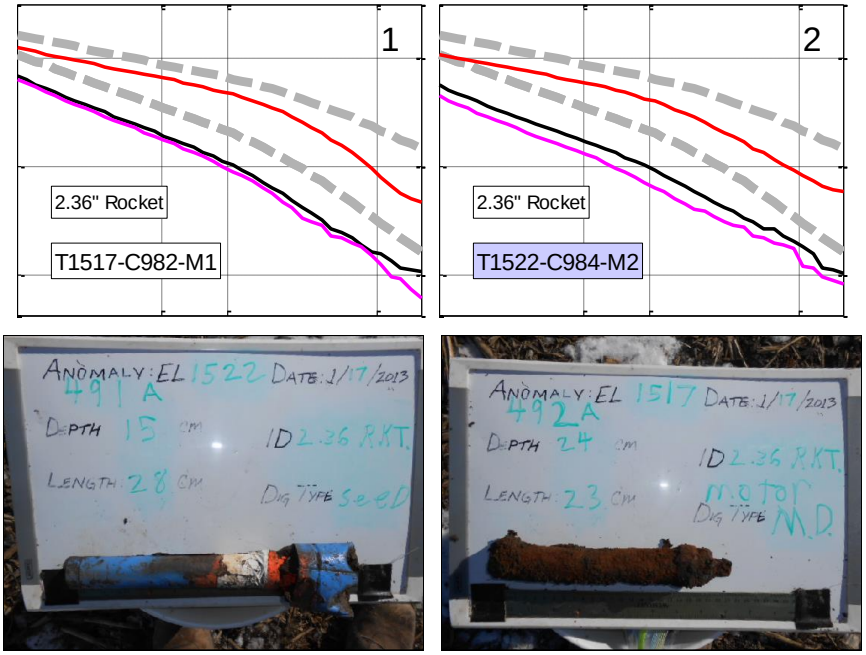

Figure 23: Left: polarizabilities and ground truth for EL-1522 (2.36" rocket). Right: polarizabilities and ground truth for EL-1517 (2.36" rocket motor).

b. Description of how the analysis procedures have been modified based on the additional information provided

We have created reference polarizabilities based on the two missed TOI. Adding these to our ordnance reference library will ensure that items with similar polarizabilities will be dug.

c. Evidence that the modified analysis scheme correctly classifies the missed seeds and can reasonably be expected to correctly classify all remaining TOI.

Adding polarizabilities based on the two missed TOI to our ordnance reference library ensures that if these items were to be classified (and not treating them as training items) they would all occur before our stop dig point (in fact at digs 58 and 94, respectively, for EL-132 and EL-1522). Our augmented reference library also ensures that other items with sufficiently similar polarizabilities will be found.

- - - - End of Failure Analysis Memo - - - -

Applying the changes to our classification process as outlined in the failure memo required that we dig several more anomalies relative to the stage 1 list. The stop dig point for the stage 2 list was set at dig 206. Other than using a new ordnance library, the classification approach remained unchanged.

The partial ROC curve for our stage 2 dig list is shown in Figure 24. The partial ground truth received with the scoring of the stage 2 dig list did not reveal any new TOI classes. Based on the ground truth, a number of variants in the ordnance library were removed, while a new variant of the 2.36" rocket was added. Table 5 lists all of the ordnance items in reference library used when creating the final (stage 3) dig list. Figure 25 shows the fifteen ordnance items in the reference library.

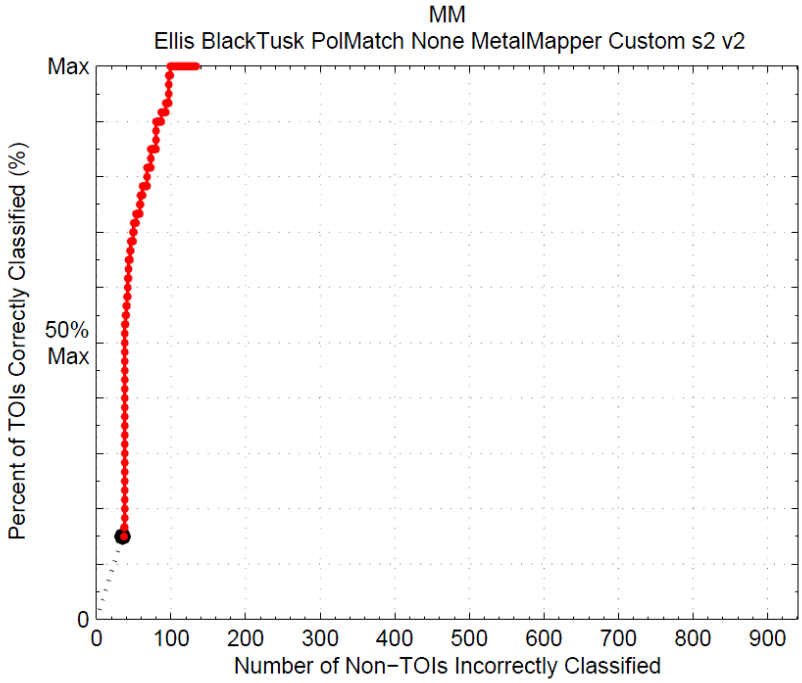

Figure 24: Partial ROC curve for the stage 2 dig list.

Table 5: List of ordnance items in the reference library used in creating the final dig list

	Name	Size (mm)
1	2.36" Rocket	60
2	2.36" Rocket B	60
3	2.36" Rocket C	60
4	2.36" Rocket D	60
5	Al. RG A	50
6	Al. RG B	50
7	Hand Grenade	70
8	Hand Grenade B	70
9	Hand Grenade C	40
10	Hand Grenade D	40
11	Rifle Grenade	50
12	Small ISO	52
13	Steel RG A	50
14	Steel RG B	50
15	Steel RG D	50

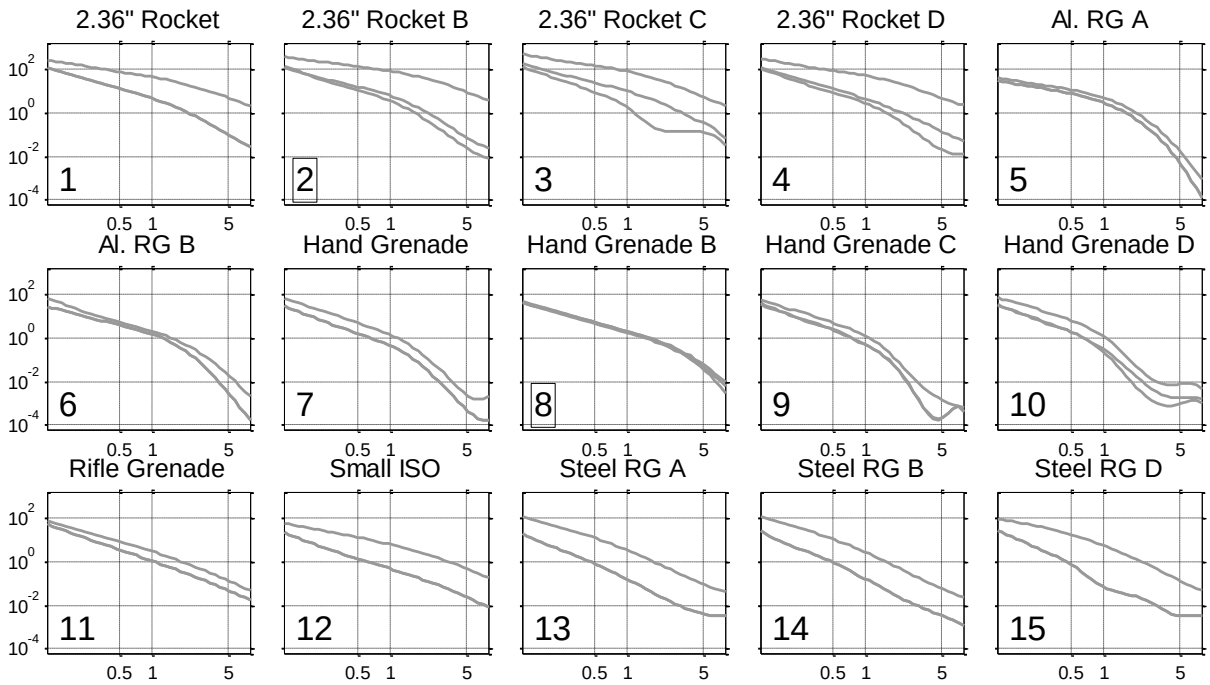

Figure 25: Ordnance library used to create the final (stage 3) dig list.

Inspection of the polarizabilities of the anomalies after the stage 2 stop dig point suggested that, with high confidence, all TOI resembling the items in our ordnance library had been dug. As a safety measure we decided to add a small number "QC digs". Rather than digging the next N anomalies on our stage 2 dig list, we selected, for each class of TOI, the two or three anomalies after the stop dig point with the best fitting polarizabilities (with respect to the library polarizabilities). These items were manually moved up on the dig list; our final (stage 3) dig list thereby had 13 additional digs relative to the stage 2 list. With one additional item classified as "cannot analyze", the stop dig point on the stage 3 list was dig number 220. The partial ROC curve for our stage 3 dig list is shown in Figure 26. All 13 additional QC digs were non-TOI. Based on this result, we decided to stop digging.

The final dig list missed one TOI (see Figure 27): EL-941, a rifle grenade at 19 cm depth, which occurred at dig number 587. We dug 220 items (207 unique items after removing shared anomalies) to find 60 of 61 TOI, which, ignoring the one missed TOI, gives a FAR of 2.45 non-TOI digs per TOI dig.

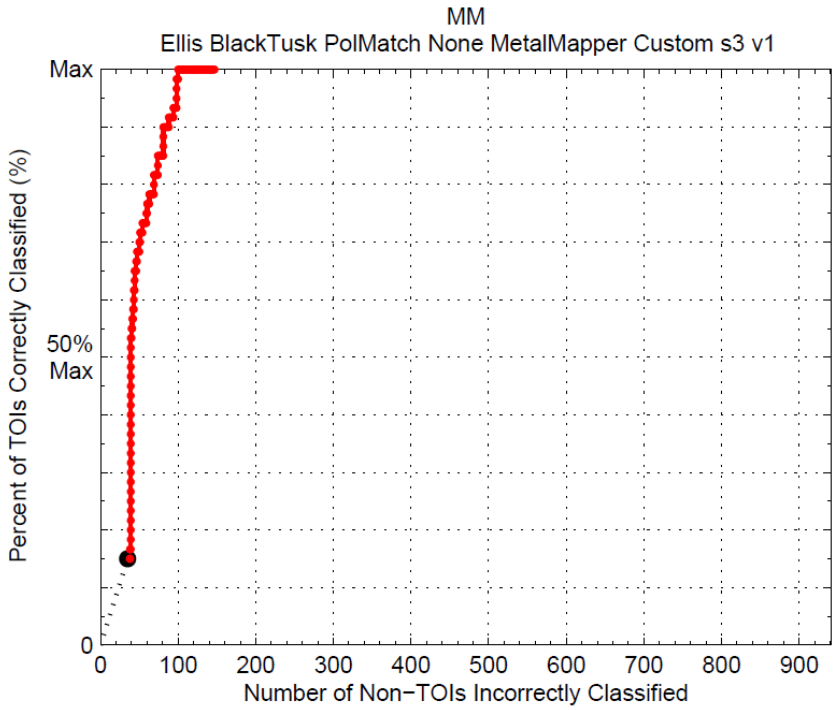

Figure 26: Partial ROC curve for the stage 3 (final) dig list.

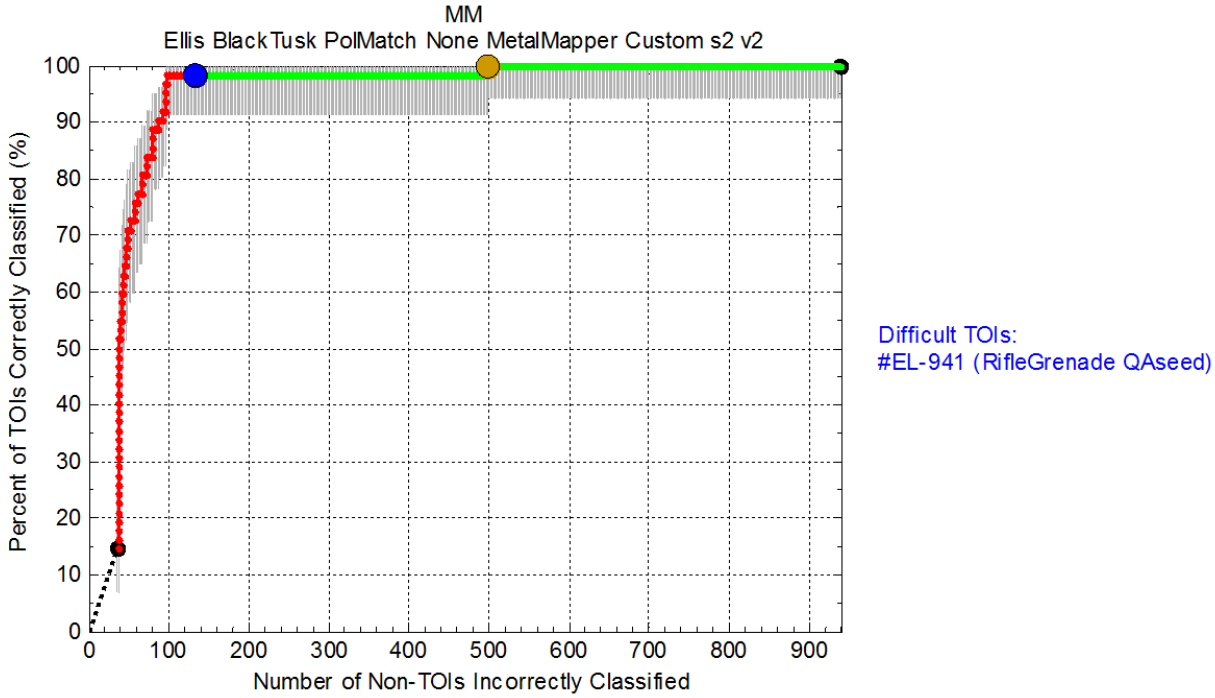

Figure 27: Final ROC curve. One missed TOI (EL-941, rifle grenade 19cm deep) was dug at dig number 587.

MetalMapper static retrospective analysis

Missed TOI: EL-941

Our final dig list missed one TOI: (1) EL-941, a rifle grenade at 19cm depth. Polarizabilities and ground truth photo for EL-941 are shown in Figure 28. Relative to the best matching reference library item the polarizability misfit value (0.626) is quite large, hence its occurrence at dig number 587 on our dig list. The best fitting reference item ("Steel RG D") was based on EL-132, which was one of the two missed QC seeds from stage 1.

For EL-132 we chose two of the multi-object inversion models for the basis of a new library reference item ('Steel RG D") because these two models were consistent and provided the best fit to an existing rifle grenade reference item ("Steel RG A", which was based on test pit measurements; Figure 29). In fact, if we had chosen the SOI model, EL-941 would have appeared much earlier on our dig list. Figure 30 shows the polarizabilities for EL-941 plotted against a reference item based on the SOI model for EL-132. Note the much lower polarizability misfit value (0.283 versus 0.626), which is low enough so that EL-941 would have appeared near our stop dig point, and would likely have been dug. An additional factor that may have contributed to our missing EL-941 is that, relative to the rifle grenade used in the IVS and test pit, and relative to the seed item EL-132, the seed rifle grenade at EL-941 is not intact, missing both part of its head and the tail fins. Thus, in a sense, this object could be considered a "one-off" item. Such items are typically more difficult to find.

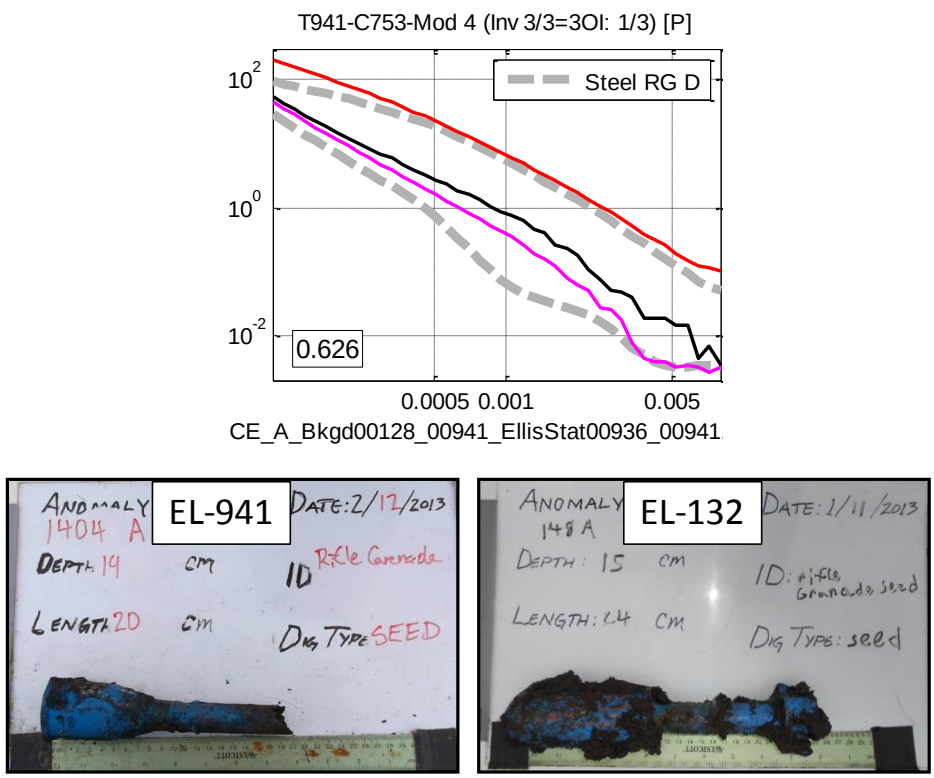

Figure 28: Left: polarizabilities for missed TOI EL-941 (colored lines), a rifle grenade at 19 cm depth, and the best fitting rifle grenade reference polarizabilities ("Steel RG D", which was based on EL-132: broken grey lines). Center: ground truth photo for El-941. Note that the rifle grenade is not intact. Right: ground truth photo for EL-132. Note that this rifle grenade is intact.

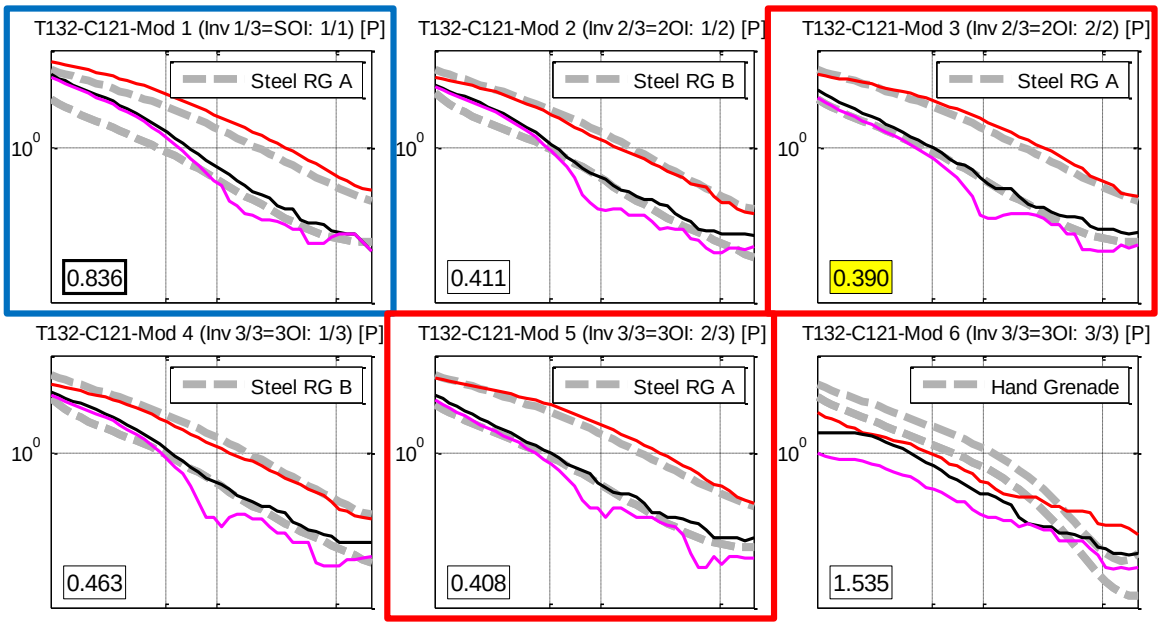

Figure 29: Polarizabilities for missed QC seed EL-132 (colored lines) plotted against the best fitting reference items available during the creation of the stage 1 dig list. Top left: SOI model; Top center and right: 2OI models; Bottom row: 3OI models. Models highlighted in red show the models that were used to construct our "Steel RG D" reference item. If instead we had created a reference model based on the SOI model (highlighted in blue), EL-941 would have been dug much earlier.

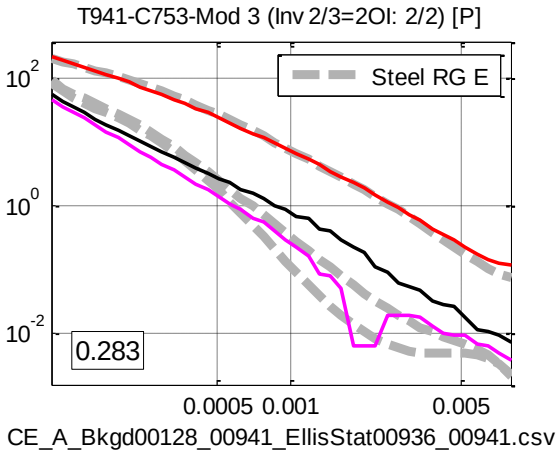

Figure 30: Polarizabilities for missed TOI EL-941 (colored lines) plotted against a reference item ("Steel RG E") based on the SOI model for EL-132.

Small ISO consistency as measure of site difficulty

Small ISOs have been used as seed items at a number of recent Live Site demonstrations: Camp Beale (2011), Pole Mountain (2011) and Spencer (2012). The consistency of the recovered polarizabilities at each site can be viewed as a measure of the difficulty of each site for classification. Figure 31 shows the recovered polarizabilities for all small ISO anomalies at Camp Ellis. The overall consistency is excellent. The largest polarizability misfit value is 0.261 for EL-406, which appears at dig number 143 on our final list.

Figure 32 shows a compilation of the polarizabilities for small ISOs at recent Live Site demonstrations. The mean misfit values, calculated with respect to the best fitting reference polarizability, is a good measure of site difficulty. It is clear that of the sites shown, Beale is the most challenging. The Beale Parsons and Beale CH2M Hill data sets comprise the same set of anomalies and the data were collected using the same MetalMapper instrument. For reasons that are not totally clear, but most likely related to differences in field practices, the Beale Parsons data resulted in more consistent ISO polarizabilities than the Beale CH2M Hill data. The excellent consistency of the Pole Mountain ISO polarizabilities reflects that site's reputation as an easy site for classification. The Spencer URS ISO polarizabilities are slightly less consistent than those from Pole Mountain, suggesting it is a slightly more challenging site. The consistency of the polarizabilities for the Spencer dataset collected by NAEVA is marginally better than that of the URS dataset. The consistency of the Camp Ellis ISO polarizabilities actually exceeds that seen at Pole Mountain; however, note that the small ISOs used at Pole Mountain and Beale were slightly different (thinner walls) than the ISOs used at the other sites. Regardless, the consistency of the Ellis ISO polarizabilities is an indication of the high quality of the dataset, suggesting that classification at Ellis should be relatively easy. Our results, ignoring the one missed TOI which could have been found much earlier if a slightly different approach had been used, bears this out.

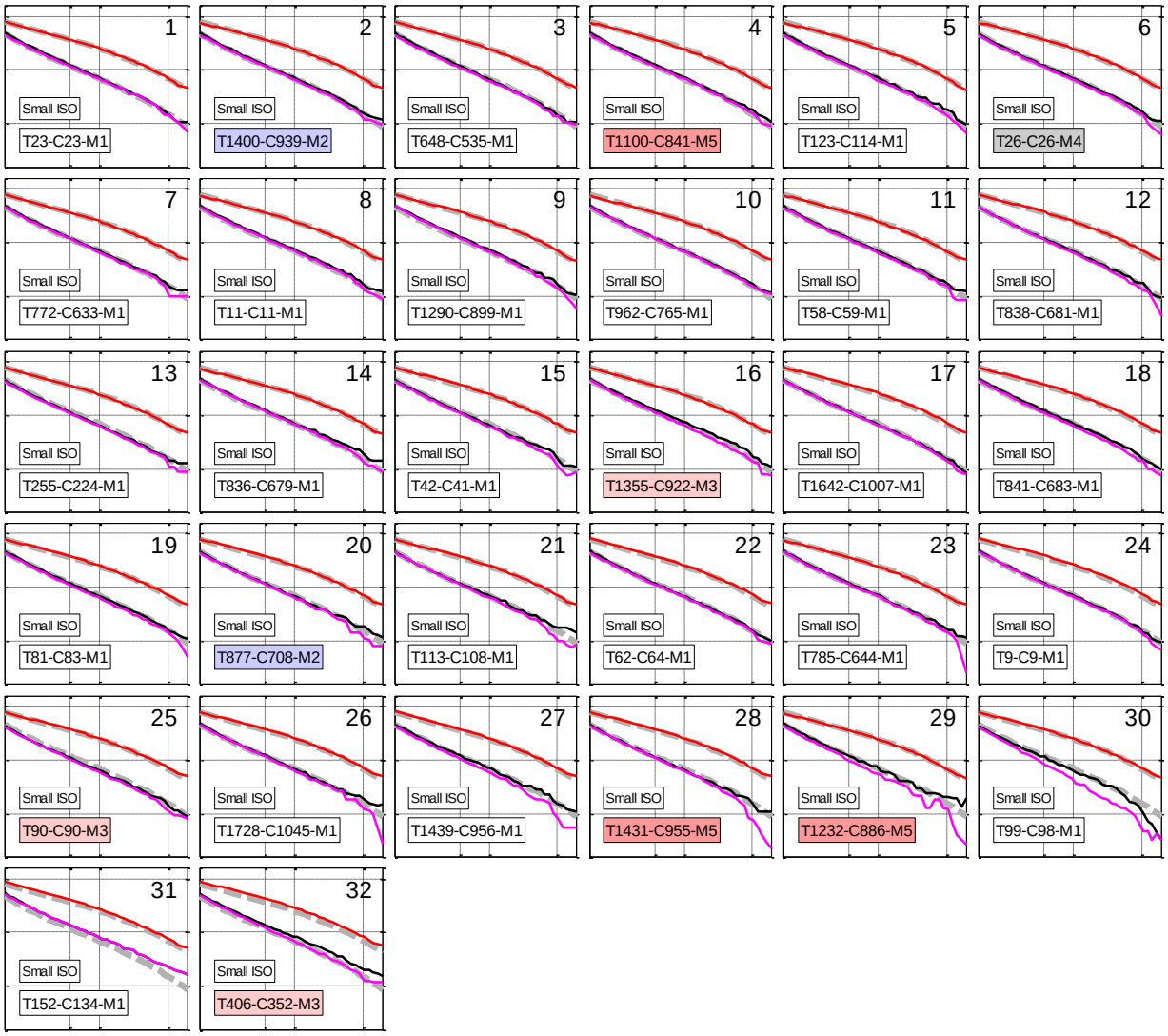

Figure 31: Polarizabilities for 32 small ISOs at Camp Ellis. Colored lines are predicted polarizabilities. Broken grey lines are small ISO reference polarizabilities taken from IVS measurements. Anomaly ID is the number after the "T" in each label. Polarizabilities are sorted by misfit (from best to worst) with respect to the small ISO reference model.

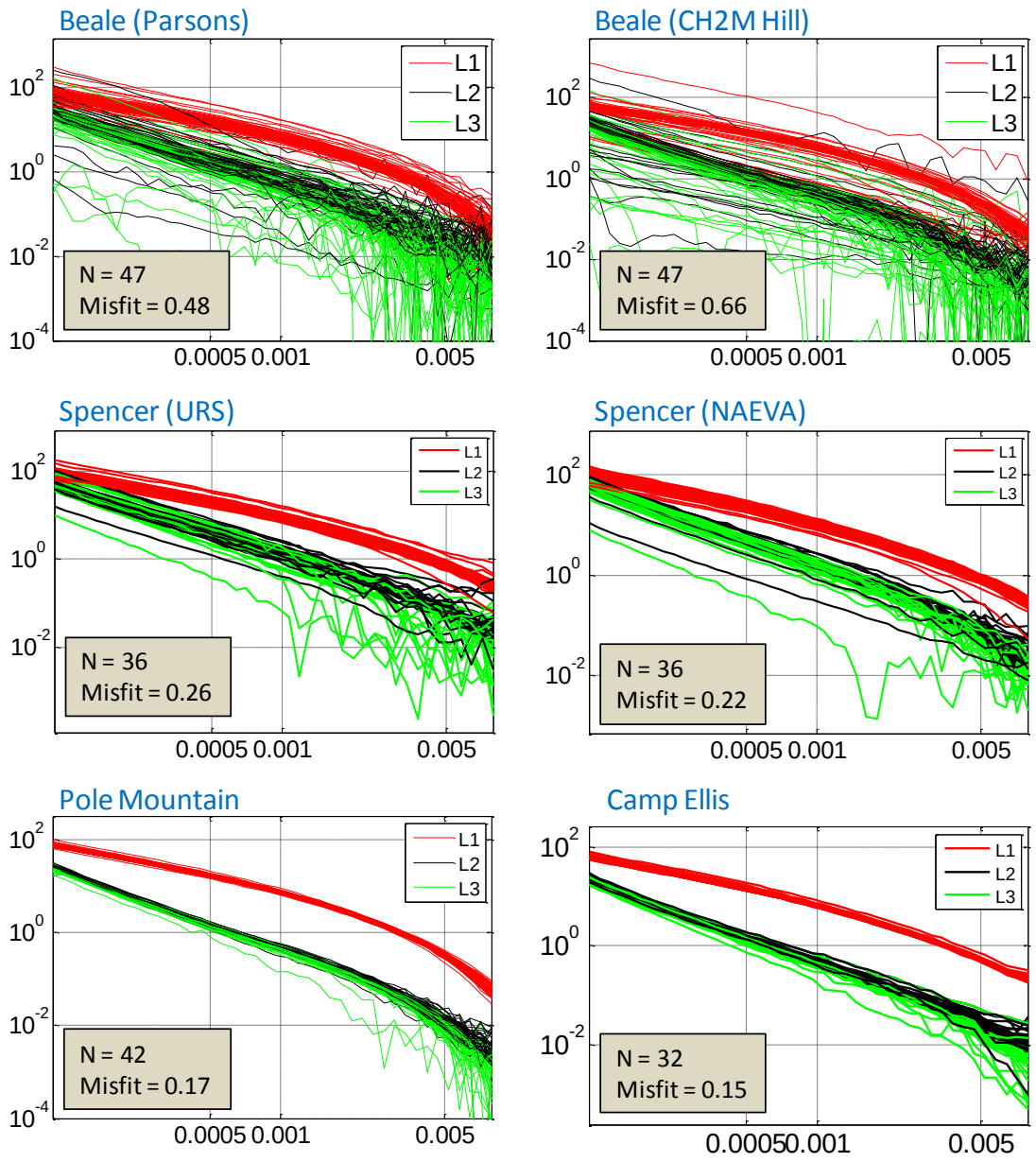

Figure 32: Compilations of polarizabilities for small ISOs from recent Live Site demonstrations. The two Beale and Spencer datasets each comprise the same set of anomalies but the data were collected by two different companies. The Spencer data include small ISOs from both the Open and Dynamic Areas. Misfit values are the mean misfits with respect to the reference polarizabilities calculated over all time channels using all three polarizabilities (L1, L2 and L3).

Appendix B: MetalMapper Polarizability Match to Targets of Interest

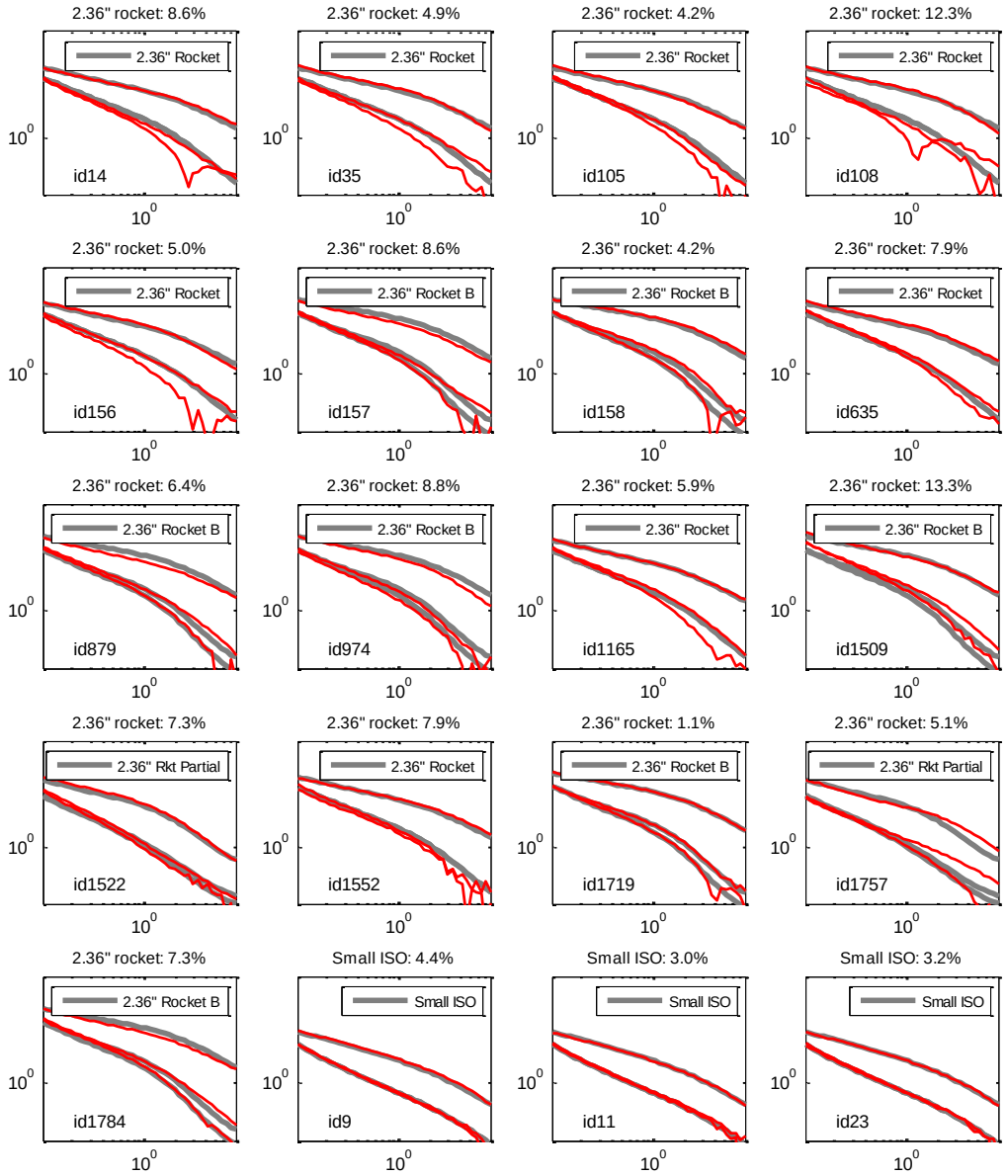

Figure 33: MetalMapper polarizability matching to TOI. The grey curve represents the TOI polarizabilities from the reference library and the red curve depicts the best matching recovered polarizabilities. The title of each plot lists the ground truth as well as the percent error between the library reference item and the recovered polarizabilities.

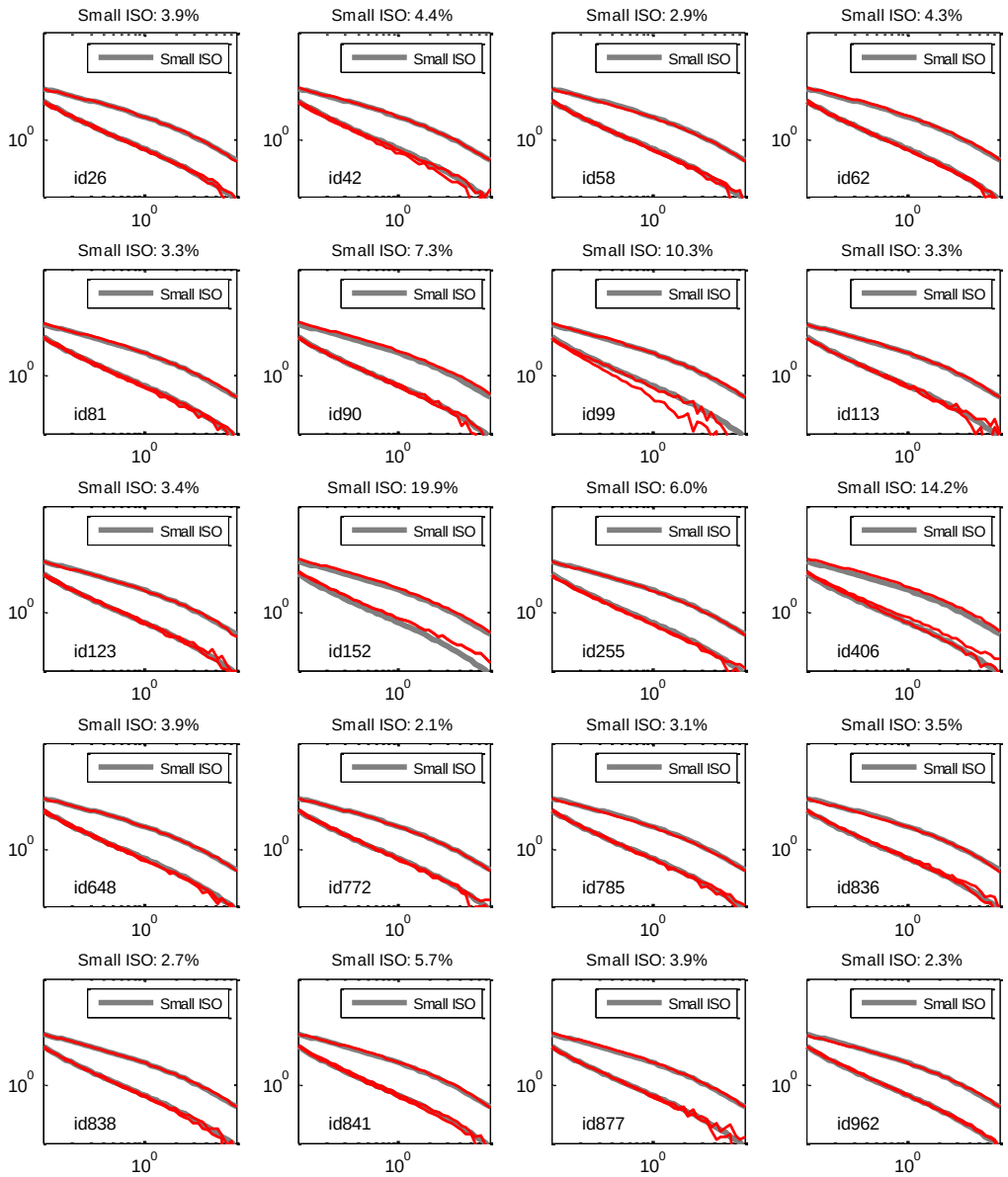

Figure 34: MetalMapper polarizability matching to TOI. The grey curve represents the TOI polarizabilities from the reference library and the red curve depicts the best matching recovered polarizabilities. The title of each plot lists the ground truth as well as the percent error between the library reference item and the recovered polarizabilities.

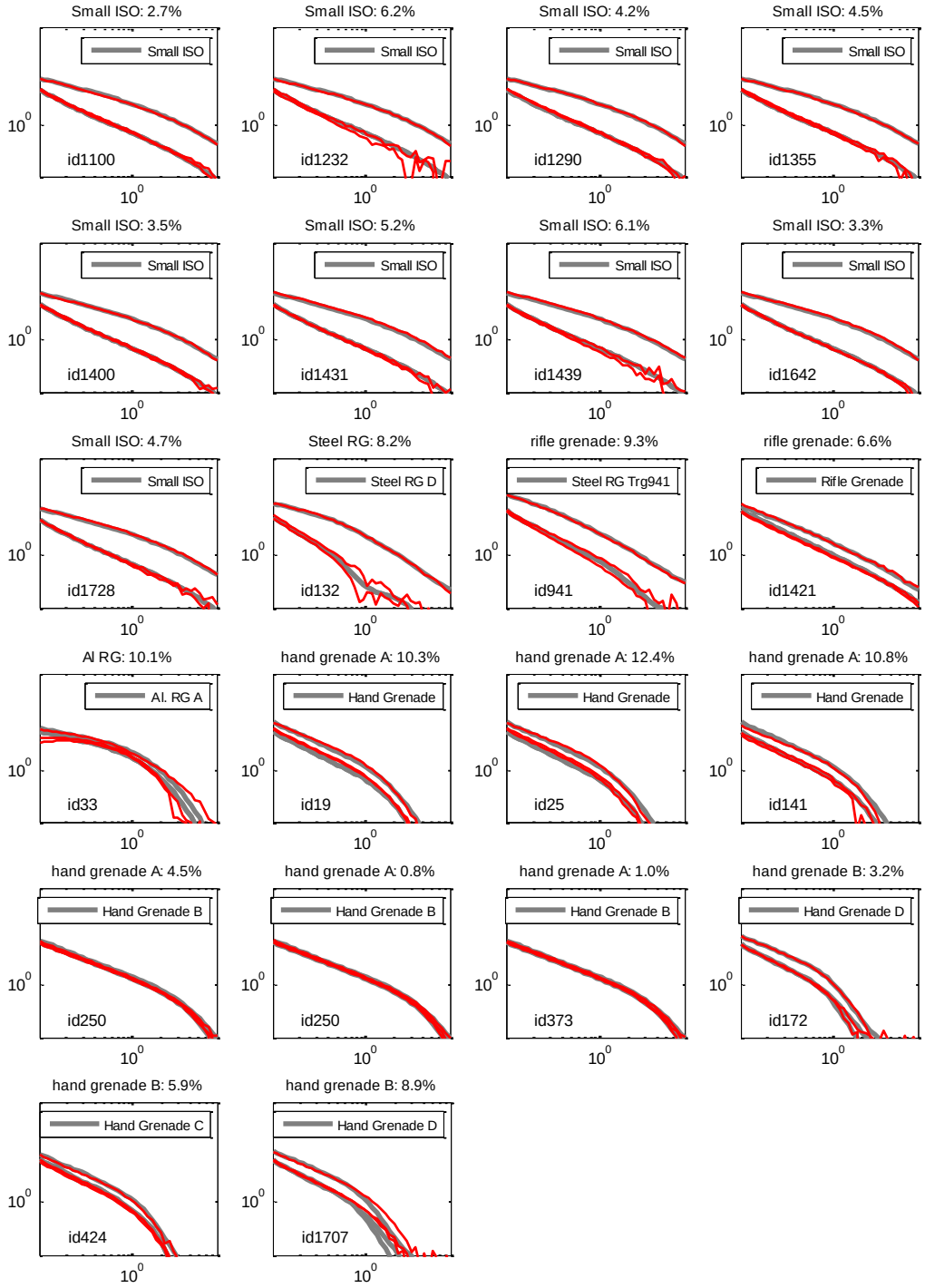

Figure 35: MetalMapper polarizability matching to TOI. The grey curve represents the TOI polarizabilities from the reference library and the red curve depicts the best matching recovered polarizabilities. The title of each plot lists the ground truth as well as the percent error between the library reference item and the recovered polarizabilities.

Table 6: Recovered polarizability accuracies relative to the best matching reference library item for Camp Ellis MetalMapper dataset.

Ground Truth	ID	%diff	Library reference
2.36" rocket	14	8.6	2.36" Rocket
2.36" rocket	35	4.9	2.36" Rocket
2.36" rocket	105	4.2	2.36" Rocket
2.36" rocket	108	12.3	2.36" Rocket
2.36" rocket	156	5	2.36" Rocket
2.36" rocket	157	8.6	2.36" Rocket B
2.36" rocket	158	4.2	2.36" Rocket B
2.36" rocket	635	7.9	2.36" Rocket
2.36" rocket	879	6.4	2.36" Rocket B
2.36" rocket	974	8.8	2.36" Rocket B
2.36" rocket	1165	5.9	2.36" Rocket
2.36" rocket	1509	13.3	2.36" Rocket B
2.36" rocket	1522	7.3	2.36" Rkt Partial
2.36" rocket	1552	7.9	2.36" Rocket
2.36" rocket	1719	1.1	2.36" Rocket B
2.36" rocket	1757	5.1	2.36" Rkt Partial
2.36" rocket	1784	7.3	2.36" Rocket B
Small ISO	9	4.4	Small ISO
Small ISO	11	3	Small ISO
Small ISO	23	3.2	Small ISO
Small ISO	26	3.9	Small ISO
Small ISO	42	4.4	Small ISO
Small ISO	58	2.9	Small ISO
Small ISO	62	4.3	Small ISO
Small ISO	81	3.3	Small ISO
Small ISO	90	7.3	Small ISO
Small ISO	99	10.3	Small ISO
Small ISO	113	3.3	Small ISO
Small ISO	123	3.4	Small ISO
Small ISO	152	19.9	Small ISO
Small ISO	255	6	Small ISO

Ground Truth	ID	%diff	Library reference
Small ISO	406	14.2	Small ISO
Small ISO	648	3.9	Small ISO
Small ISO	772	2.1	Small ISO
Small ISO	785	3.1	Small ISO
Small ISO	836	3.5	Small ISO
Small ISO	838	2.7	Small ISO
Small ISO	841	5.7	Small ISO
Small ISO	877	3.9	Small ISO
Small ISO	962	2.3	Small ISO
Small ISO	1100	2.7	Small ISO
Small ISO	1232	6.2	Small ISO
Small ISO	1290	4.2	Small ISO
Small ISO	1355	4.5	Small ISO
Small ISO	1400	3.5	Small ISO
Small ISO	1431	5.2	Small ISO
Small ISO	1439	6.1	Small ISO
Small ISO	1642	3.3	Small ISO
Small ISO	1728	4.7	Small ISO
Steel RG	132	8.2	Steel RG D
rifle grenade	941	9.3	Steel RG Trg941
rifle grenade	1421	6.6	Rifle Grenade
Al RG	33	10.1	Al. RG A
hand grenade A	19	10.3	Hand Grenade
hand grenade A	25	12.4	Hand Grenade
hand grenade A	141	10.8	Hand Grenade
hand grenade A	250	4.5	Hand Grenade B
hand grenade A	250	0.8	Hand Grenade B
hand grenade A	373	1	Hand Grenade B
hand grenade B	172	3.2	Hand Grenade D
hand grenade B	424	5.9	Hand Grenade C
hand grenade B	1707	8.9	Hand Grenade D

Appendix C: MetalMapper Location and Depth Error Estimates

In this section, we present location and depth estimate error distributions calculated for targets of interest in the MetalMapper dataset. All data soundings were considered in this analysis. That is, if an anomaly flag has multiple data anomalies acquired, depth and location estimates from all the data inversions are included in the statistics.

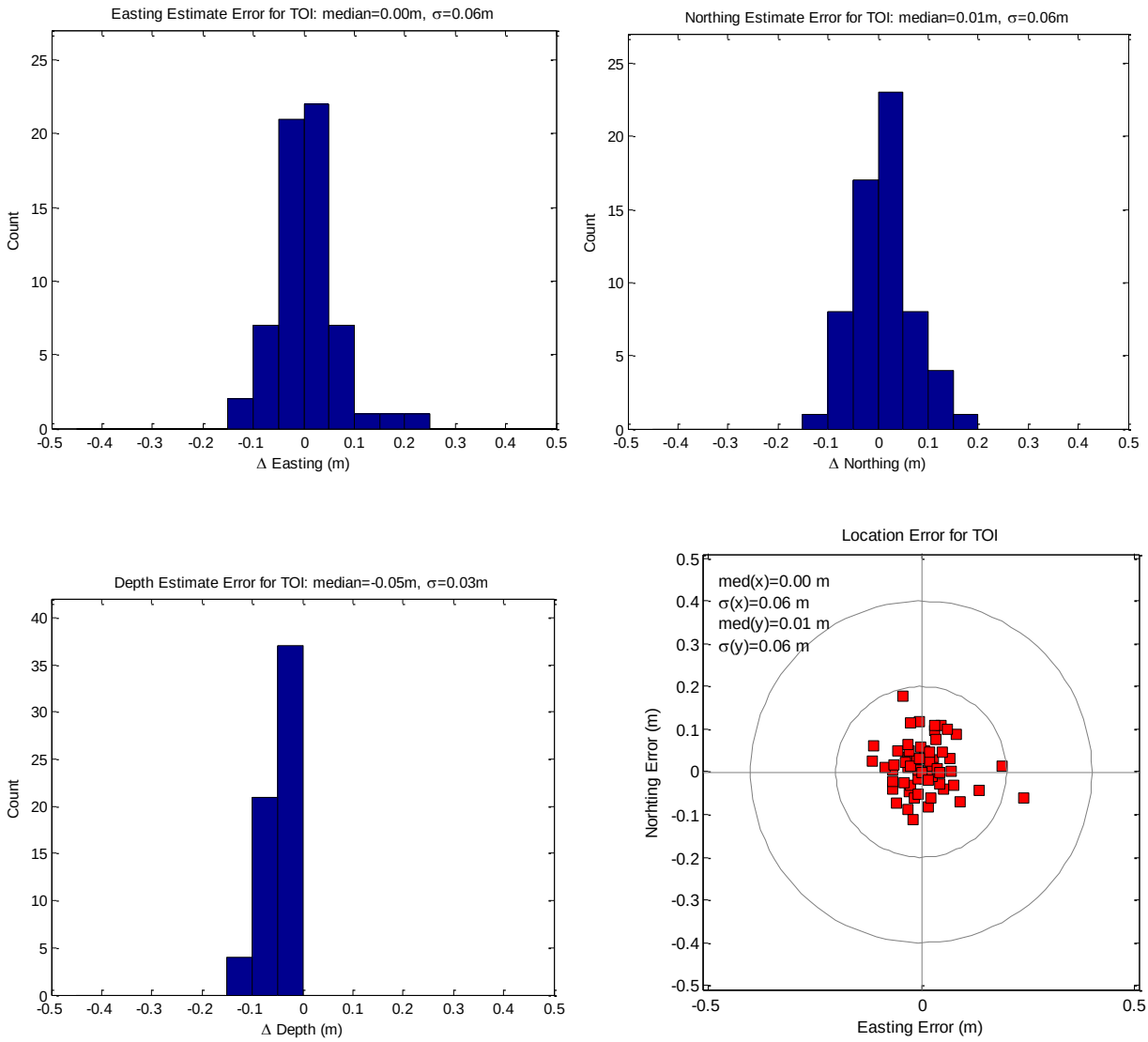

Figure 36: Location and depth error distributions.

Appendix D: TEMTADS 2x2 Feature Extraction and Classification

NOTE: The discussion contained in this section is relative to the submitted dig list. Note that in the ESTCP scoring results, some targets are removed. Differences in the total number of targets, stop dig point, etc will occur between the analyses described below for the submitted dig list with analysis of final scoring results which have shared targets removed.

I. Overview

In the Camp Ellis demonstration, there were 1077 TEMTADS 2x2 cued anomalies for classification. The inversions were run with single, two, and three-object models. A visual QC process was conducted with special attention paid to several metrics of misfit, data SNR, and recovered polarizabilities. The classification task was performed primarily using a library matching method based on how well target polarizabilities matched a set of reference TOI library polarizabilities. All three polarizabilities (primary, secondary, tertiary) were used to calculate the polarizability misfit (ϕ_m) between a test anomaly and a reference TOI. The minimum ϕ_m value for each test anomaly against all reference items is used to rank the anomalies. The library matching method consists of four parts: 1) building a polarizability library; 2) assessment of the matching level of test polarizabilities with respect to a set of reference polarizabilities; 3) training requests; 4) producing a ranked anomaly list and classification. The polarizability library, which initially is built using the provided test pit and IVS data would be updated based on information ascertained from training or intermediate dig.

The dataset was divided into five subsets which approximately reflect the confidence level of each anomaly, ranging from "high likelihood" TOI to "likely clutter" (see Table 7). Further, the anomalies were also categorized into a number of reference class sets in which each anomaly is marked with a matching level. In this process, features such as size, decay rate, depth range, and skewness (a measure of the degree of non-spherical deviation developed in SERDP MR-2318) of polarizabilities were considered to identify if there were some other "suspicious" spherical and rod-like objects at the training stage. In each reference class set, a Recursive Ordering Similarity Matrix (ROSM) algorithm was applied to reorder anomalies based on self-similarity. In a reordered reference class set, a group of similar anomalies or a single unique anomaly can be more easily recognized.

Table 7: TEMTADS 2x2 Evaluation of Matching Levels at Camp Ellis

Set		Number of Anomalies	Dig (Training, Can't Analyze)	Dig-TOI	Dig-Frag
HTOI	High confidence TOI	21	21(7, 0)	13	8
LTOI	Likely TOI	295	57(28, 0)	18	39
LLTOI	Low likelihood TOI	230	57(27, 0)	5	52
LVLTOI	Very low likelihood TOI	95	20(11, 0)	1	19
LC	Likely clutter	436	26(20, 0)	0	26
	Total	1077	181(93, 0)	37	144

II. Classification Result

Initial polarizability matching was based on IVS measurements and selected reference polarizabilities from previous sites. In addition to the TOI classes identified in the IVS, there were a number of items with polarizabilities similar to those of a warhead and rocket motor. In particular, there were a large number of items whose recovered polarizabilities were unique and fairly consistent which were identified through training as rocket weights. Figure 37 shows some types of anomalies that were requested as training data.

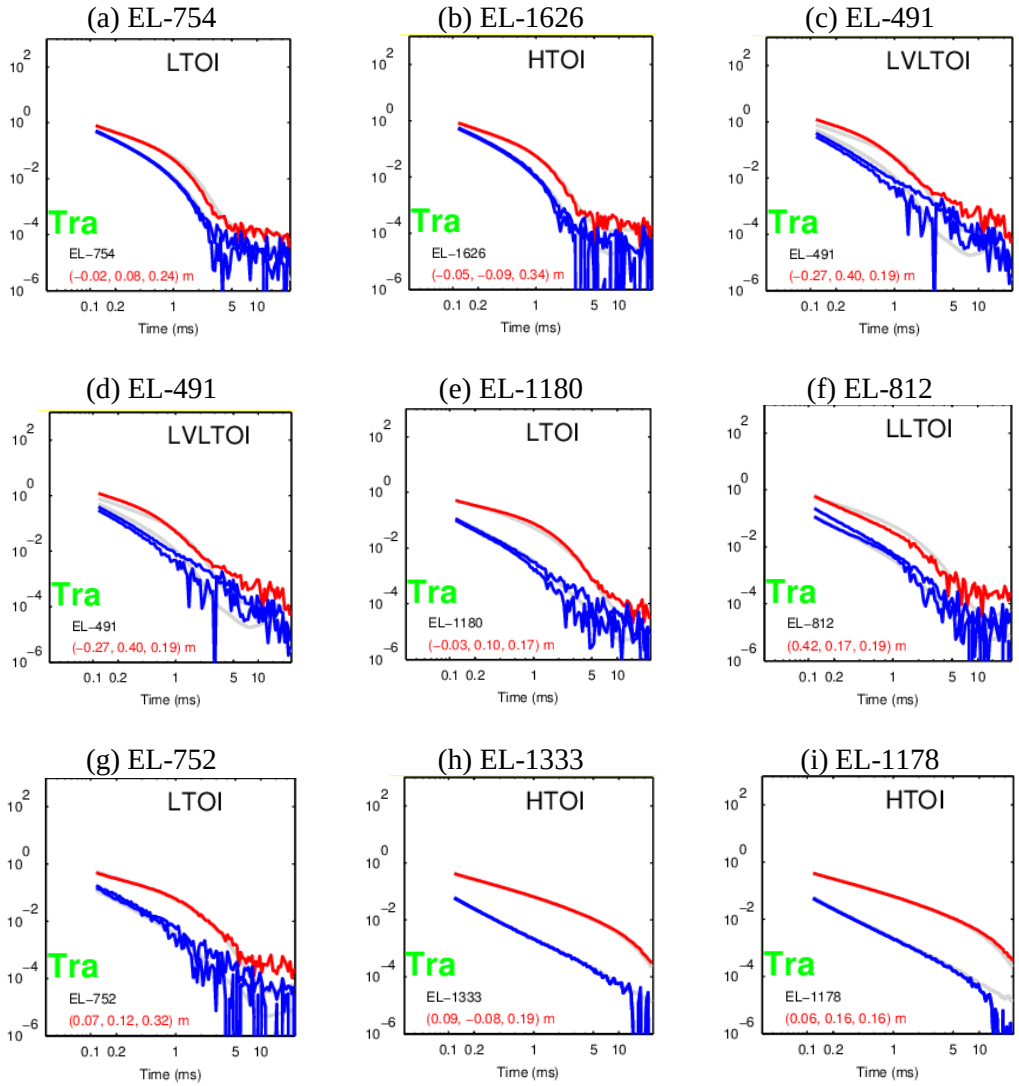

Figure 37: The polarizabilities of some suspicious anomalies in the training stage, War head: (a)-(c), rocket motor: (d)-(f) and rocket weight: (g)-(h).

From the information extracted from the IVS and training data, seven reference polarizability classes were created: 1) 2.36″ Rocket; 2) ISO80; 3) Rifle Grenade; 4) Hand Grenade; 5) Warhead; 6) Rocket Motor; 7) Rocket Weight (non-TOI). Figure 38 presents the TOI reference polarizabilities from IVS and training data. In each reference class, there might be more than one set of polarizabilities in order to account for variations.

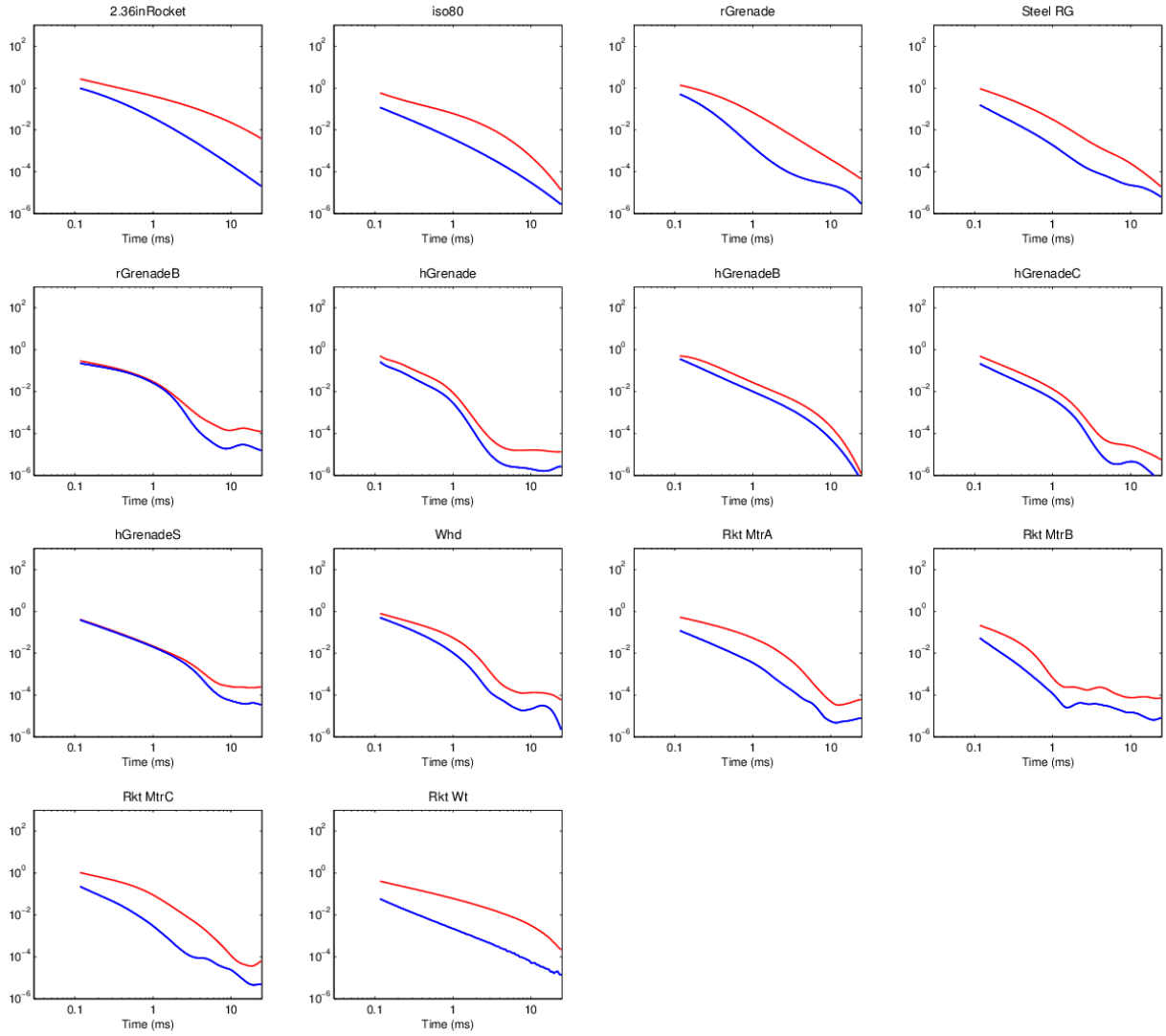

Figure 38: Seven reference classes used in the library matching method for the classification of TEMTADS 2x2 data at Camp Ellis.

The classification was conducted in four stages. In stage 1, there no items were assigned to "Can't extract reliable parameters" (CANT) class. The training data suggested that the 497 anomalies assigned to the class of rocket weight (Rkt Wt) were very likely non-TOI and were therefore labeled as non-TOI. These non-TOI rocket weights comprise roughly 46% of the total anomalies. For the items assigned to the classes of Warhead and Rocket Motor, all related training requests were designated non-TOIs. However, a conservative approach was taken, and some anomalies related to these classes were marked to be dug as

there can be unknown small TOIs that might fall into these two reference classes. This conservative approach was validated by the ground truth that was received and some TOI were found in the warhead/rocket motor classes. Unfortunately, there are many such similar items and, even with a conservative approach, one QC seed was missed in stage 1. The missed seed was assigned to the class of Rocket Motor (see analysis below). After making corrections to ensure that items similar to this seed would be dug, a modified stage 1 dig list was submitted as stage 2. Based on the missed QC seed and the available ground truth, searching for potential Grenade-type TOI (Figure 39) became an important task in stages 3 and 4.

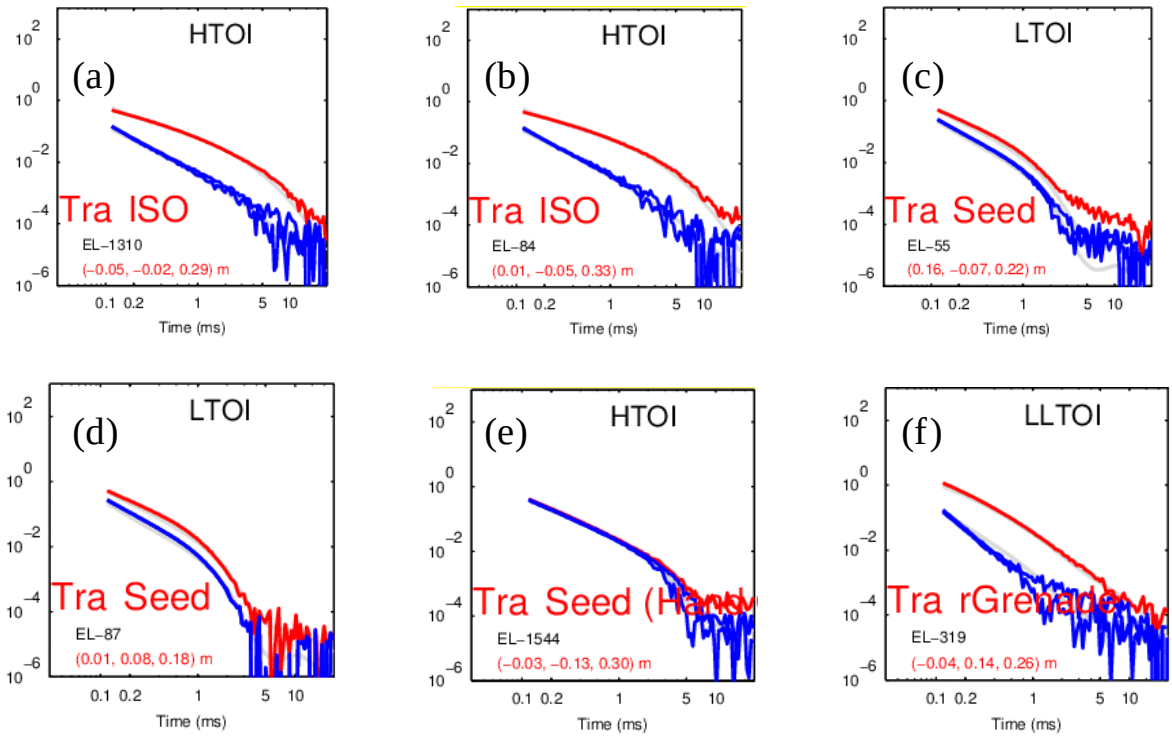

Figure 39: Polarizabilities of six TOI found in the training stage. Small ISO: (a)-(b). Hand Grenade: (c)-(e). Rifle Grenade: (f).

Table 7 lists the evaluation of 1077 anomalies in terms of matching level. The HTOI set contained 21 anomalies, LTOI 295, LLTOI 230, LVLTOI 95, and LC 436. Among the total anomalies, HTOI anomalies take up about 2%. This gives an estimate of the number of likely TOI in the dataset. All 21 HTOI anomalies were dug, of which 13 were TOI. In the LTOI set, 57 digs contained 18 TOI. In the LLTOI set, 57 digs contained 5 TOI. In the sets of low likelihood TOI (LVLTOI, LC), the 46 digs found only one TOI.

Table 8 summarizes the performance at each stage. In stages 1 and 2, 30 TOI were found out of 72 dug anomalies. In stages 3 and 4, 11 and 5 anomalies were marked as 'Dig', respectively. All of these were non-TOIs. In the final submitted dig list, the total number of digs, including training anomalies, was 181. 37 of 38 TOI were dug. Approximately 86% of the non-TOI items were correctly labeled as non-TOI. Figure 40 shows the ROC curve from stage 4 and lists the one missed item. Analysis of the missing TOI follows in the next section.

Table 8: Summary of TEMTADS 2x2 classification result at Camp Ellis.

Category/Stage	Labeled	TOI	Frag
Training	93	7	86
CANT	0	0	0
Stages 1 and 2	72	30	42
Stage 3	11	0	11
Stage 4	5	0	5
Total Dig	181	37	144
Non-dig	896	1	895 (86%)
Total anomalies	1077	38	1039

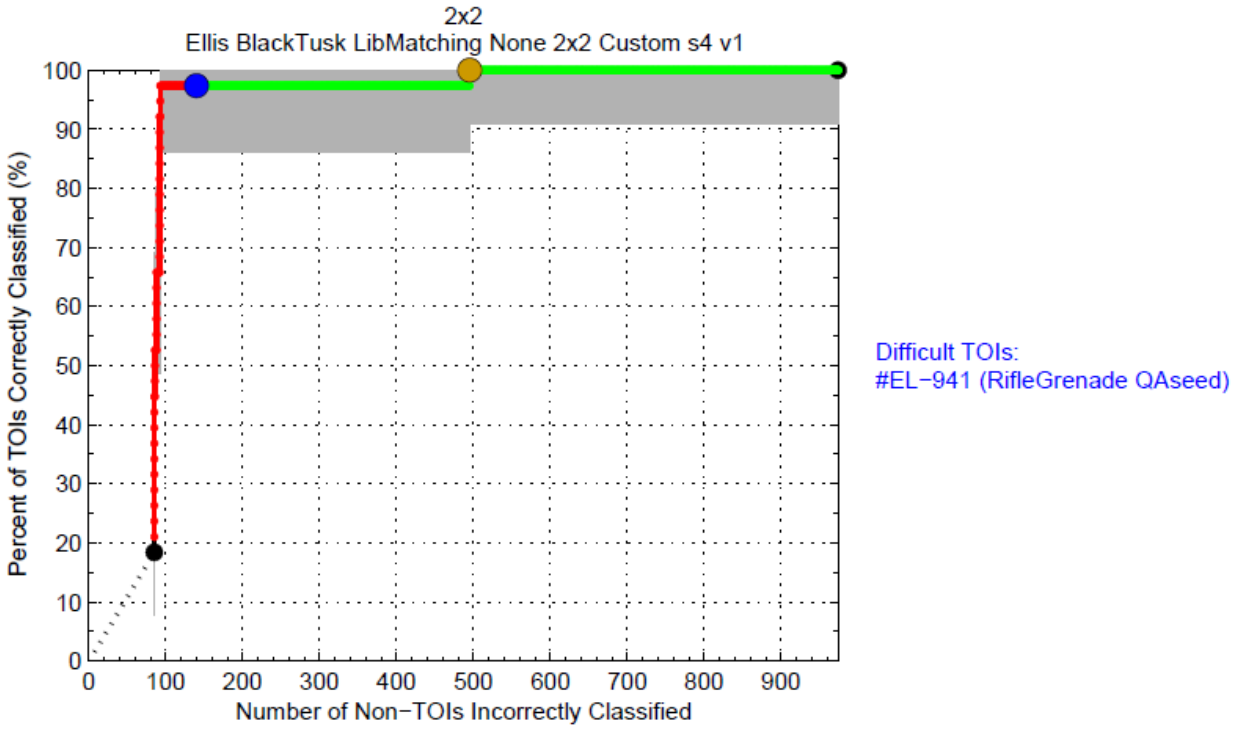

Figure 40: Final ROC curve (stage 4) for TEMTADS 2x2 cued data. One TOI was missed.

III. Missed TOI

1. One QC seed

In the stage 1 dig list, one QC seed was not marked to be dug (EL-143). The ground truth for this anomaly is a Hand Grenade with a piece of 2.36in Rocket Motor and one piece of 2.36in Rocket Weight (see Figure 41(a)).

For each anomaly, single, two, and three-object inversions were performed producing six sets of recovered polarizabilities. All models were ranked based on the misfit (ϕ_m) between a test anomaly polarizability and a reference TOI polarizability. A set of polarizabilities which had the minimum ϕ_m value for each test anomaly against all sets of reference items was selected for classification analysis. Figure 41(b) shows that the polarizabilities used for the analysis are an excellent match to the Rocket Motor A from the reference library. There are no polarizability features matching a reference hand Grenade or any of the requested training TOI shown in Figure 41(d)-(e). For this anomaly, other sets of polarizabilities were reviewed and the only set of polarizabilities that remotely matches a hand grenade (shown in Figure 41(c)) is noisy and does not provide a good enough match to any reference polarizabilities to mark EL-143 for digging. In the training stage, ground truth information was requested for some relevant anomalies based on matches to hand Grenade polarizabilities. Figure 41(f)-(g) show the polarizabilities of these non-TOI training anomalies. Because these training anomalies were non-TOI, the QC seed, which has similar polarizabilities, was not marked to be dug in order to mitigate potentially excessive false alarms.

In the training stage, ground truth requests were made for similar anomalies to EL-143. Figure 42 shows the three requested similar anomalies (EL-812, EL-752 and EL-1180). In fact, EL-143 was also in this small group (eight items) and caught the analyst's attention. Unfortunately, three other items in the group were selected for training requests rather than EL-143. If all these items were requested for training, EL-143 would have been dug. In stage 1, two similar anomalies (EL-427 and EL-457) in this class were dug however ground truth revealed both to be non-TOI.

Based on information received from the missed QC seed and training data we have learned that whenever there is a two or more matching anomalies of interest, all should either be dug or requested as training data to ensure the maximum probability of digging all TOI anomalies.

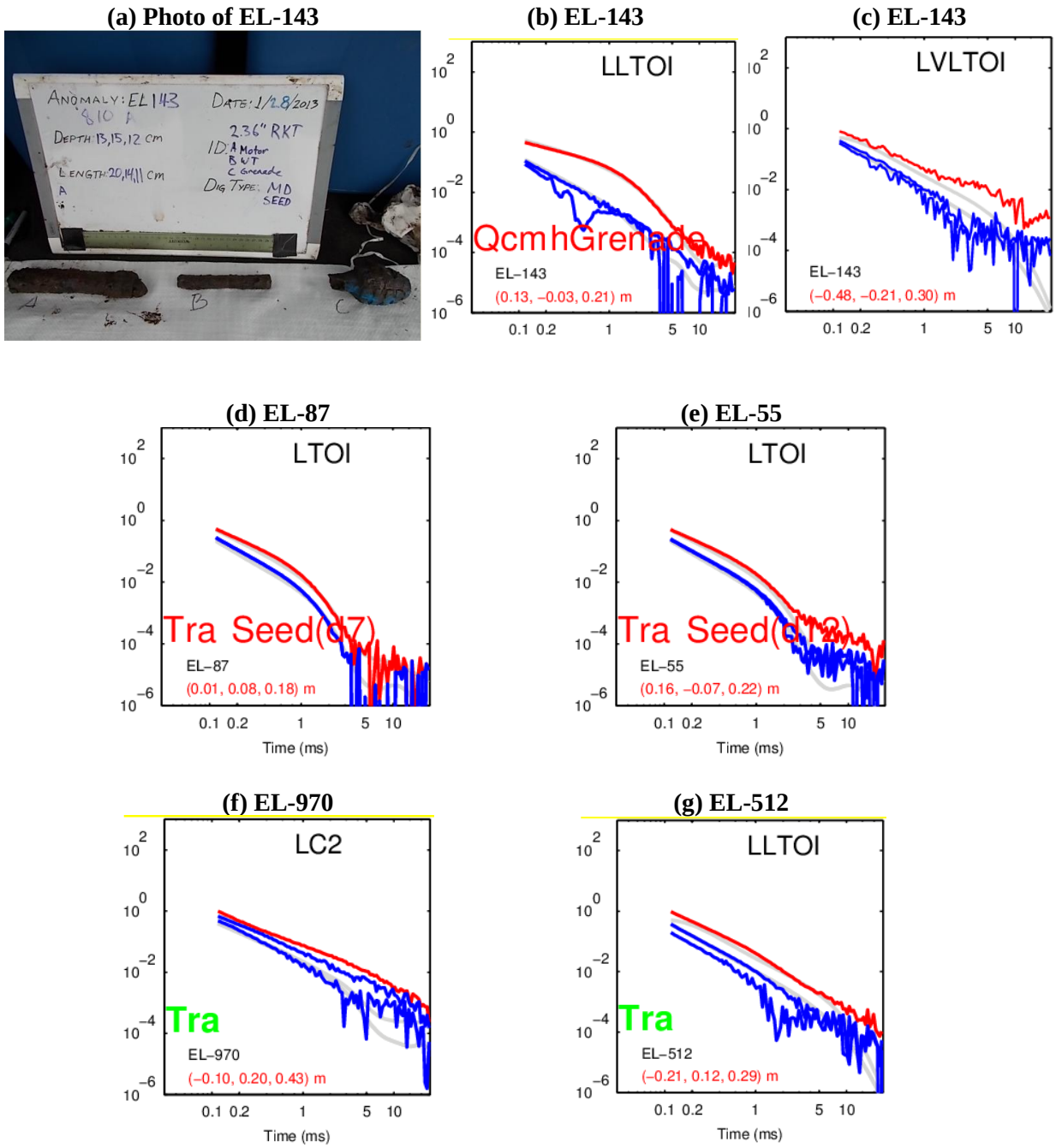

Figure 41: Missed QC seed EL-143: (a) Ground truth photo; (b) The test polarizabilities (red and blue curves) used for classification (grey curve is best matching library reference named RktMtrA); (c) the best matching polarizabilities for EL-143 that match the hand grenade reference polarizabilities; (d)-(e): recovered polarizabilities for two different targets (EL-87, EL-55) which provided high quality matches to the reference hand grenade. (f)-(g): Two other requested training anomalies (EL-970, EL-512 (non-TOIs) with polarizabilities similar to those shown for EL-143 in (c) relative to the library reference hand grenade.

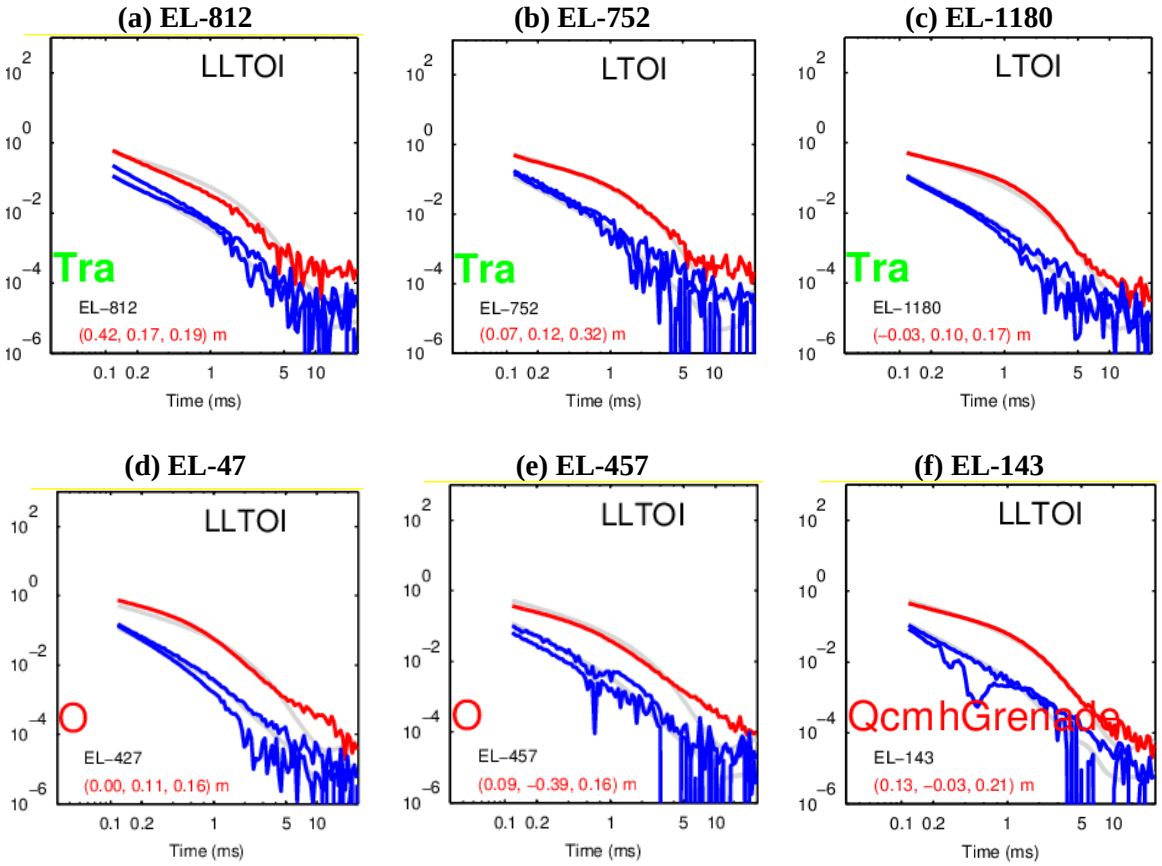

Figure 42: Polarizabilities of training anomalies (a) –(c) which were revealed to be munitions debris (EL-812) and 2.36" rocket motors (EL-752, EL-1180) and the two digs (d)-(e) in stage 1 similar to the missed QC seed EL-143 (f). Ground truth showed that none of the targets in (a)-(e) were TOI, leading to the decision to consider (f) a likely non-TOI rocket motor.

2. One QA seed

The missed QA seed is anomaly EL-941, which is a rifle grenade (Figure 43(a)). There are six other anomalies with similar polarizabilities illustrated in Figure 43(c)-(h) that are grouped together with EL-941 in this class. Only one of these similar anomalies, EL-539 (Figure 43(c)), was requested as a training anomaly. More attention during training was given to the anomalies with a slow decay after 3 ms, like those shown in Figure 43(i)-(k). It was thought that since these slow-decay training anomalies were all revealed to be non-TOI, the other faster decaying anomalies in Figure 43(c)-(h) (including EL-941) were even more likely to be non-TOI and therefore no further training requests or digs relating to the anomalies shown in Figure 43(a)-(h) were made. Because EL-941 so closely resembled the non-TOI training items, it was missed. As suggested for the case of the missed QC seed, a more conservative approach would be to request training for all of the small number of similar anomalies in Figure 43(b)-(h).

During the classification process we experimented with using matching against some non-TOI reference items (e.g., Rocket Weight and Rocket Motor) as a way to exclude non-TOI items from being dug. In the original library, the recovered polarizabilities of EL-941 were best matched against the non-TOI RktMtrC and it was not selected amongst the non-TOI training anomalies. If the RktMtrC items was removed from the library, would EL-941 have been dug?

In the Rifle Grenade Class, there were three sets of related reference polarizabilities: 1) Steel RG; 2) rGrenade; 3) rGrenadeB. In the original Rifle-Grenade class group, there were two anomalies (EL-1182 and EL-1139) marked as “rGrenade” that were requested for training. Both were non-TOI. If the reference RktMtrC is retrospectively removed from the reference library, there would be 9 additional “rGrenade” anomalies assigned to the Rifle-Grenade class group. Among them, the first three “rGrenade” anomalies would be ordered as shown in Figure 44(a)-(c). Previous experience from the Fort Rucker Live Site demonstration demonstrated the difficulty in finding hand and rifle grenades, and because of this it is quite likely that at least the top three “suspicious Grenade” anomalies would be selected for training data. Thus EL-941 would not have been missed and the remaining additional “suspicious Grenade” anomalies would also be dug. Clearly, the reference library used for classification can have a significant impact on decisions related to dig/no-dig and training/no-training requests.

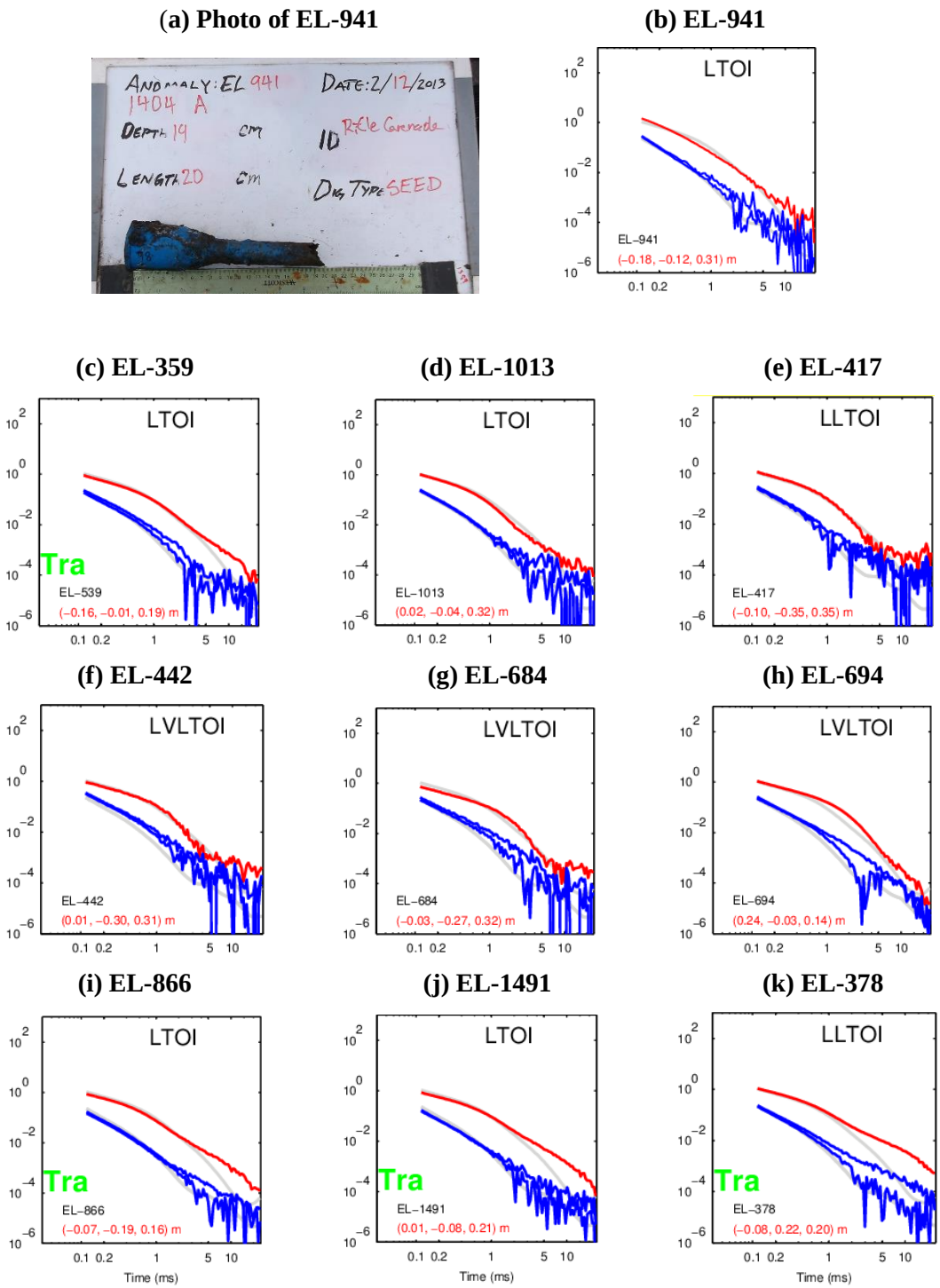

Figure 43: Missed QA seed EL-941 and related, similar non-TOI. (a) El-941 photo. (b) Test polarizabilities (red and blue curves) used for classification and best matching referenceitem (RktMtrC). (c)-(h) Similar non-TOI anomalies adjacent to EL-941. (i)-(k) non-TOI training anomalies with a slow decay after 3 ms relative to anomalies in (b)-(h).

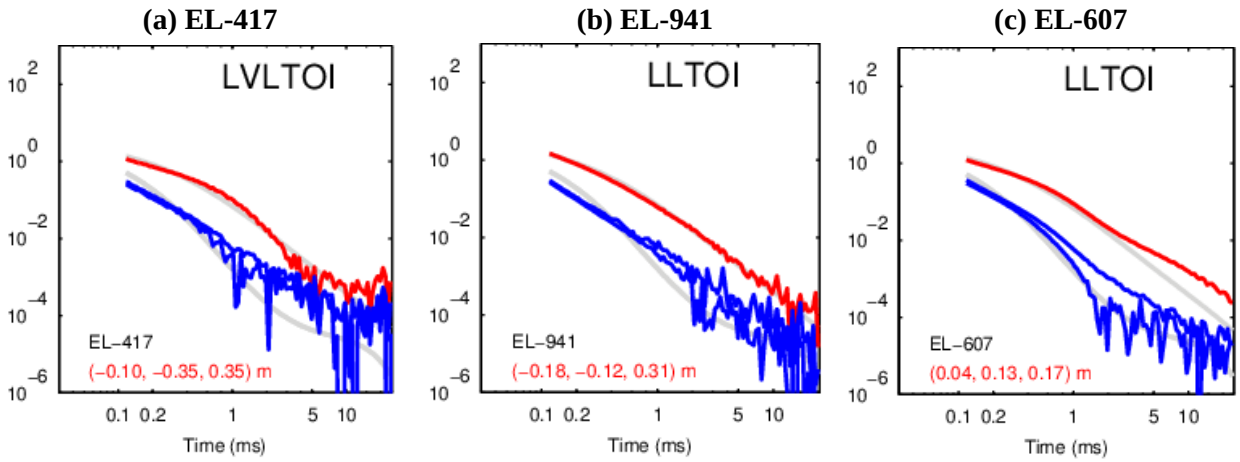

Figure 44: A Rifle Grenade class group obtained after removing RktMtrC from the reference library: EL-417, missed QA seed EL-941 and EL-607 are marked as the first three "rGrenade" anomalies. They would most likely be requested as the most "suspicious Grenade" anomalies in the training process. Thus EL-941 would be caught at the expense of digging a few more non-TOI.

Appendix E: TEMTADS 2x2 Polarizability Match to Targets of Interest

NOTE: Target EL-645 was removed from the final anomaly list.

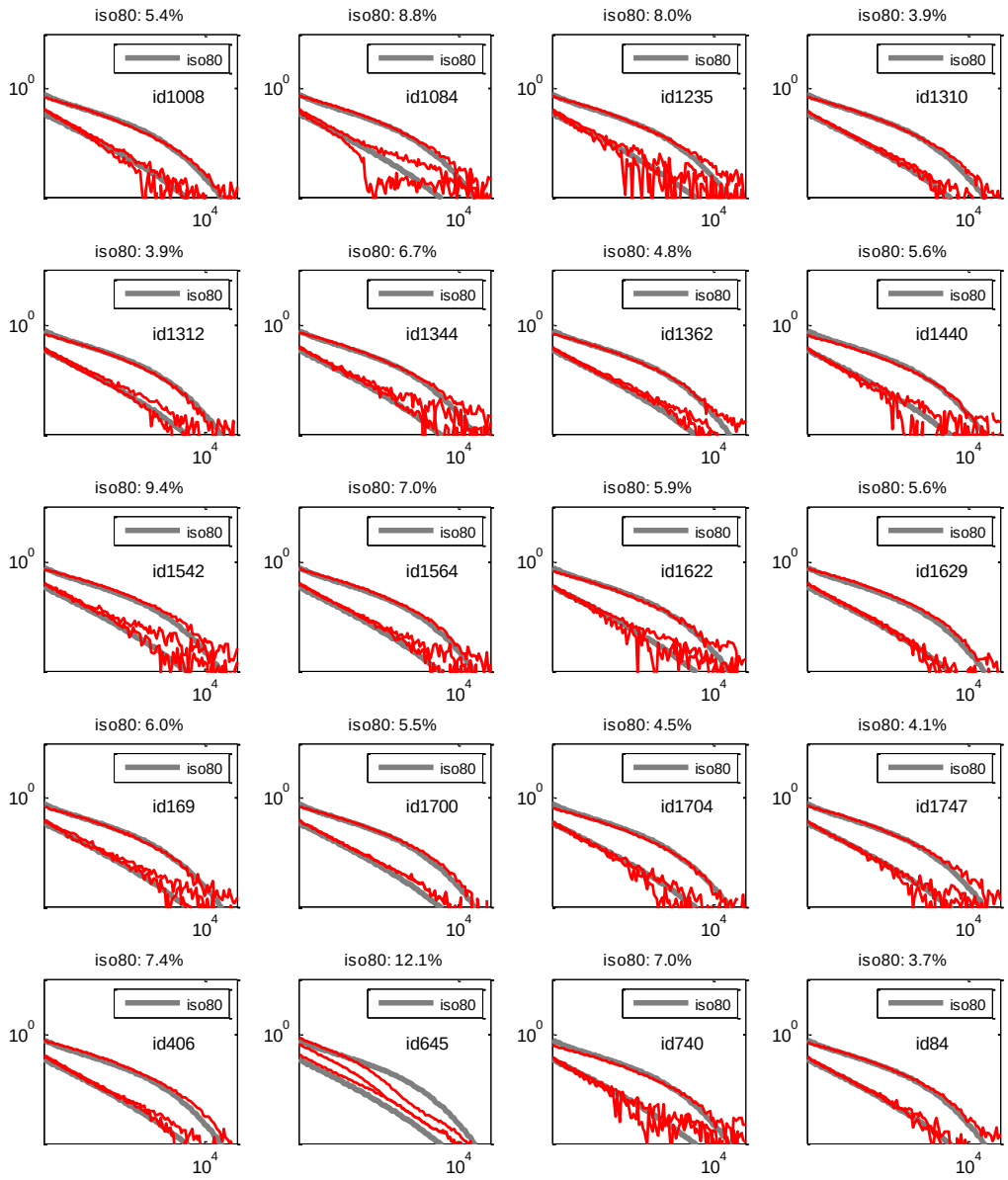

Figure 45: TEMTADS 2x2 polarizability matching to TOI. The grey curve represents the TOI polarizabilities from the reference library and the red curve depicts the best matching recovered polarizabilities. The title of each plot lists the ground truth as well as the percent error between the library reference item and the recovered polarizabilities.

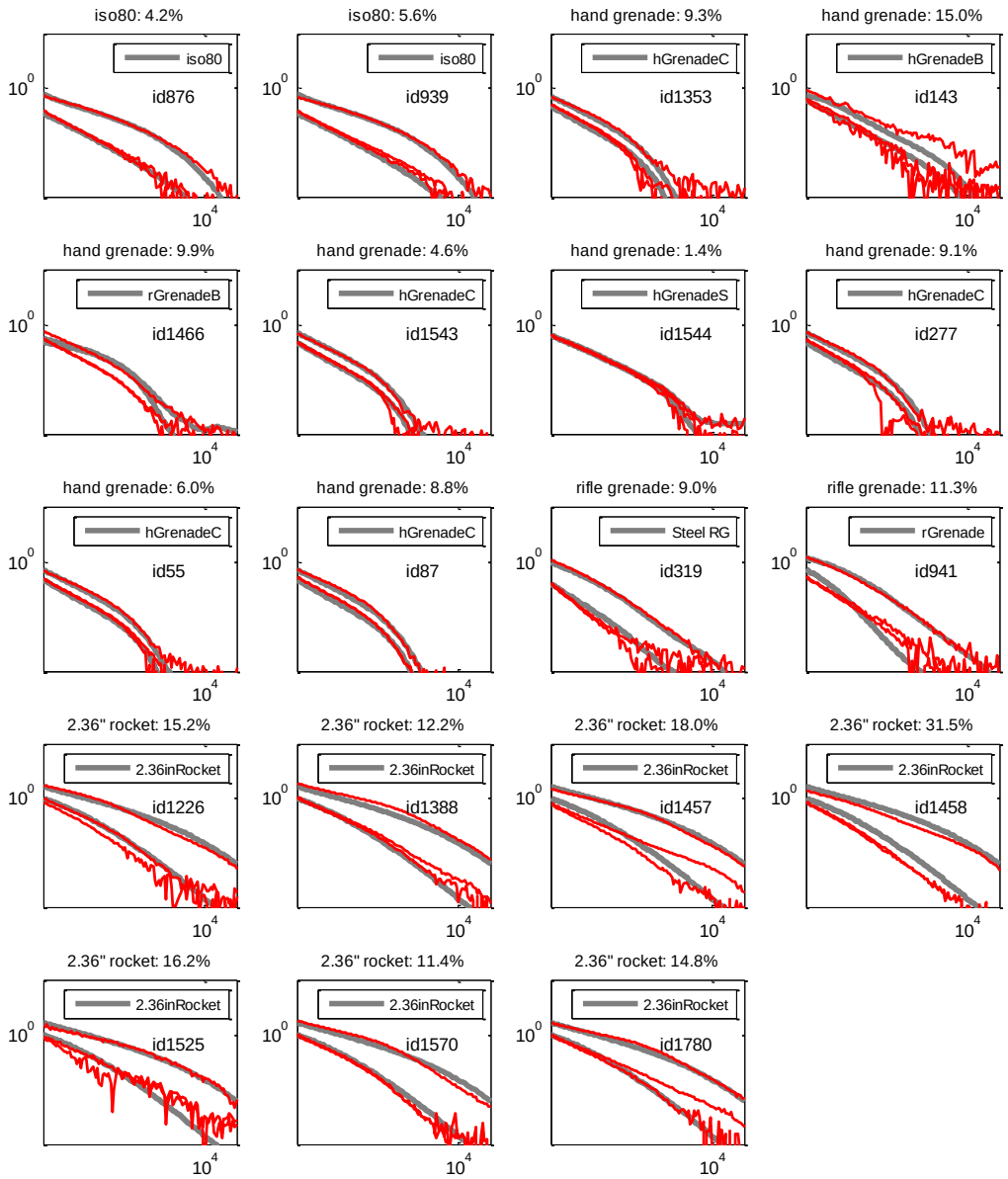

Figure 46: TEMTADS 2x2 polarizability matching to TOI. The grey curve represents the TOI polarizabilities from the reference library and the red curve depicts the best matching recovered polarizabilities. The title of each plot lists the ground truth as well as the percent error between the library reference item and the recovered polarizabilities.

Table 9: Recovered polarizability accuracies relative to the best matching reference library item for TEMTADS 2x2.

Ground Truth	ID	%diff	Library reference
iso80	1008	5.4	iso80
iso80	1084	8.8	iso80
iso80	1235	8	iso80
iso80	1310	3.9	iso80
iso80	1312	3.9	iso80
iso80	1344	6.7	iso80
iso80	1362	4.8	iso80
iso80	1440	5.6	iso80
iso80	1542	9.4	iso80
iso80	1564	7	iso80
iso80	1622	5.9	iso80
iso80	1629	5.6	iso80
iso80	169	6	iso80
iso80	1700	5.5	iso80
iso80	1704	4.5	iso80
iso80	1747	4.1	iso80
iso80	406	7.4	iso80
iso80	645	12.1	iso80
iso80	740	7	iso80
iso80	84	3.7	iso80

Ground Truth	ID	%diff	Library reference
iso80	876	4.2	iso80
iso80	939	5.6	iso80
hand grenade	1353	9.3	hGrenadeC
hand grenade	143	15	hGrenadeB
hand grenade	1466	9.9	rGrenadeB
hand grenade	1543	4.6	hGrenadeC
hand grenade	1544	1.4	hGrenadeS
hand grenade	277	9.1	hGrenadeC
hand grenade	55	6	hGrenadeC
hand grenade	87	8.8	hGrenadeC
rifle grenade	319	9	Steel RG
rifle grenade	941	11.3	rGrenade
2.36" rocket	1226	15.2	2.36inRocket
2.36" rocket	1388	12.2	2.36inRocket
2.36" rocket	1457	18	2.36inRocket
2.36" rocket	1458	31.5	2.36inRocket
2.36" rocket	1525	16.2	2.36inRocket
2.36" rocket	1570	11.4	2.36inRocket
2.36" rocket	1780	14.8	2.36inRocket

Appendix F: TEMTADS 2x2 Depth Error Estimates

In this section, we present location and depth estimate error distributions calculated for targets of interest in the TEMTADS 2x2 dataset. All data soundings were considered in this analysis. That is, if an anomaly flag has multiple data anomalies acquired, depth and location estimates from all the data inversions are included in the statistics. The TEMTADS did not have IMU information, and therefore we do not calculate position errors for the cued TETMADS surveys.

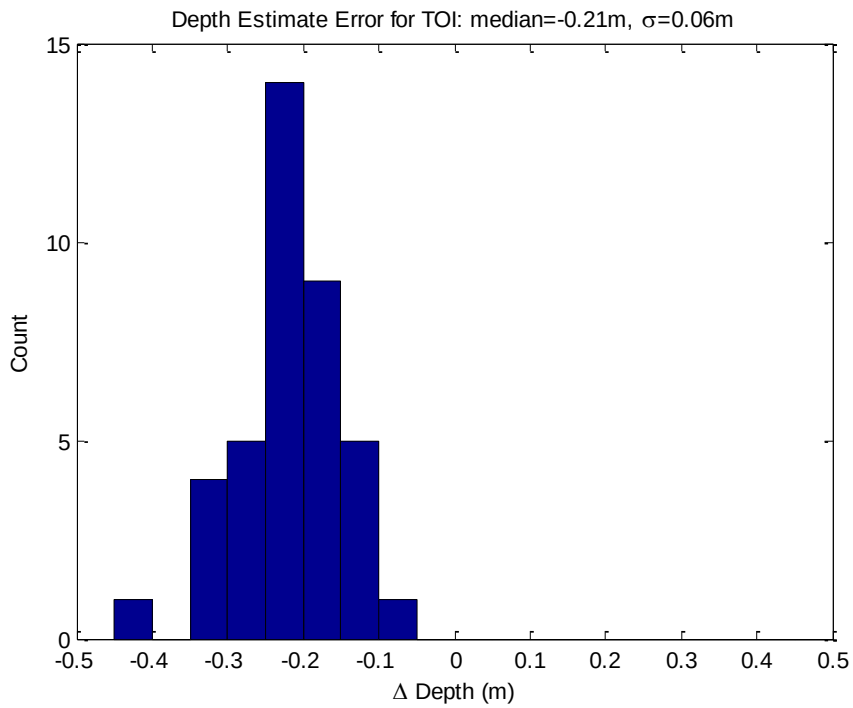

Figure 47: TEMTADS 2x2 depth error estimates for Camp Ellis. The bias in the depth errors is assumed to be a consequence of the sensor height used in the inversions differing from the actual sensor height.

Appendix G: Points of Contact

POINT OF CONTACT Name	ORGANIZATION Name Address	Phone Fax E-mail	Role in Project
Leonard Pasion	Black Tusk Geophyscics Inc, #401, 1755 W Broadway Vancouver, BC, V6J 4S5	604 428 3380 leonard.pasion@btgeophysics.com	Principal Investigator (PI), Project management and personnel coordination